

OAM beam generation in space and its applications: A review

Yudong Lian ^{a,b,*}, Xuan Qi ^{a,b}, Yuhe Wang ^{a,b}, Zhenxu Bai ^{a,b}, Yulei Wang ^{a,b}, Zhiwei Lu ^{a,b}

^a Center for Advanced Laser Technology, Hebei University of Technology, Tianjin 300401, China

^b Hebei Key Laboratory of Advanced Laser Technology and Equipment, Tianjin 300401, China



ARTICLE INFO

Keywords:

OAM beams
Intracavity generation
Extracavity conversion
OAM beams application

ABSTRACT

In recent years, vortex beams with orbital angular momentum (OAM) have attracted more and more attention. The wavefront of the OAM beams is helical, the intensity at the center of the beam is zero, and there is a phase singularity. Because of the novel phase characteristics of OAM beams, they have a wide application prospect in the fields of optical communication, rotating body detection and particle manipulation. Therefore, the research on the generation technology of OAM beams and their application range are of instructive significance to the future experiments. In this paper, the common beams carrying OAM are introduced, and the techniques of generating OAM beams in free space are summarized, including intracavity conversion method and extracavity conversion method. The application range of OAM beams studied at present is discussed, and the development trend of OAM beams is prospected. The purpose of this paper is to provide reference and guidance for related experiments of OAM beams in the future.

1. Introduction

Vortex light generally refers to the phase vortex beam, its phase or wavefront is spiral, and there is a phase singularity in the center of the beams, so the central intensity of the vortex beam is zero and the intensity distribution is annular. The common phase vortex beam is Laguerre-Gaussian beam. Because vortex beams carry orbital angular momentum, they are also called orbital angular momentum (OAM) beams. The complex amplitude expression of OAM beams in cylindrical coordinate system (r, φ, z) contains the helical phase term $\exp(il\varphi)$, where l can be any integer, which represents the topological charge of the beams, and the OAM beams with different topological charge are orthogonal to each other. The twist number and direction of the helical wavefront depend on the magnitude and the positive or the negative of l . When $l = 0$, OAM beams degenerate to Gaussian beams. In the 1950s, researchers discovered that the electric multi-stage radiation process could produce electromagnetic radiation with OAM [1]. However, in the following decades, the research on OAM of photons had been at the theoretical stage, and there was no substantial breakthrough [2,3]. Until 1992, Allen et al. found that OAM is the inherent property of vortex light with spiral wavefront and can be generated in a standard optical laboratory. Besides, the value of OAM carried by each photon in the vortex beams is integral multiple of Reduced Plank Constant [4]. At this point, people really began to study the vortex beams and their OAM. The discovery that photons can carry OAM opens up a new field of optical physics and gives people a new understanding of common

phenomena. At the same time, the research on the theory, generation, detection and application of OAM beams has become a research hotspot in the optical field at home and abroad in recent years. The research on the generation technology of OAM beams is the basis of studying properties and application fields. According to OAM beams generation mode, they can be divided into intracavity generation method and extracavity mode conversion method. The generation technology of OAM beams will be described in detail in the second chapter.

As a new type of laser beams, OAM beams are widely used in many fields. In recent years, the application of OAM beams in the field of optical communication has become one of the research hotspots in the domestic and overseas [5–8]. In the application of optical communication, the OAM of vortex beams can be used as a new coding method to encode information. It can realize mode division multiplexing and expand the capacity of optical communication like wavelength division multiplexing, time division multiplexing and polarization multiplexing [5,9,10]. In addition, mode division multiplexing can be combined with other multiplexing methods such as wavelength division multiplexing and polarization multiplexing to effectively improve the channel capacity and spectral efficiency of the optical communication system [11–13]. In addition, the rotating Doppler effect of OAM beams can be used to detect rotating bodies, including motors, rotating fluids, atmospheric vortices, etc. [14–16], which has an important application prospect in the field of measurement. Optical tweezers and optical wrenches have been developed by using OAM beams, which can capture and rotate particles without contact, and have been widely used in the field of biomedicine [17–19]. In addition to the three fields mentioned above,

* Corresponding author.

E-mail address: ydlian@hebut.edu.cn (Y. Lian).

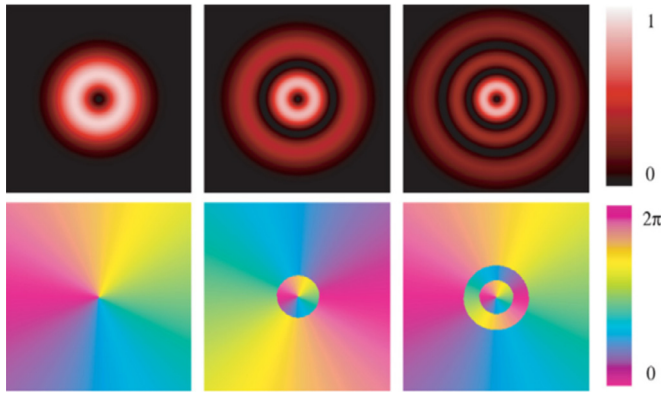


Fig. 1. The intensity and phase distributions of LG_{01} , LG_{11} and LG_{21} [22].

OAM beams are also of great application value in laser processing and super-resolution microscopic imaging [20–22].

In this paper, the methods of generating OAM beams in free space are reviewed. Starting with the theoretical introduction of three common OAM beams, several typical techniques for generating OAM beams in the cavity and outside the cavity are systematically analyzed, the application fields of OAM beams are summarized, the technical trend of generating OAM beams in free space is introduced, and the development direction of OAM beams in practical application is pointed out.

2. The common categories of oam beams

As a new type of laser beams, the OAM beams have the unique characteristics that the ordinary Gaussian beams do not have. The common beams that meet the above conditions are Laguerre-Gaussian beams, Bessel beams, Bessel-Gaussian beams, Hermite-Gaussian beams, perfect vortex beams and some novel OAM beams. This chapter will briefly introduce these OAM beams.

2.1. Laguerre-Gaussian beams

Laguerre-Gaussian beams are a kind of high-order Gaussian beams. In the cylindrical symmetric stable cavity, such as the circular aperture confocal cavity, the higher-order transverse mode is described by the product of the associated Laguerre polynomial and the Gaussian distribution function [23,24]. Therefore, the Laguerre-Gaussian beams propagating in the z direction can be expressed as [25–27]

$$LG_{pl}(r, \varphi, z) = \frac{C_{pl}}{\omega_0} \left(\frac{\sqrt{2}r}{\omega(z)} \right)^l L_p^{|l|} \left(\frac{2r^2}{\omega(z)^2} \right) \exp \left(-\frac{r^2}{\omega(z)^2} \right) \exp(il\varphi) \exp(i\theta) \quad (1)$$

Where, C_{pl} is a constant, ω_0 is the waist radius of the fundamental mode, l is the angular quantum number, p is the radial quantum number, and arbitrary non-negative integer can be taken, $\omega(z)$ and θ are respectively

$$\omega(z) = \omega_0 \sqrt{1 + \left(\frac{z}{f} \right)^2} \quad (2)$$

$$\theta = (l + 2p + 1) \tan^{-1} \frac{z}{f} - k \left(z + \frac{r^2}{2R} \right) \quad (3)$$

In the formula, $R = z + \frac{f^2}{z}$, k is the wavenumber, f is the confocal parameter, also known as Rayleigh length, and $L_p^l(\zeta)$ is the associated Laguerre polynomial [28]. The intensity and phase distributions of LG_{01} , LG_{11} and LG_{21} are shown in Fig. 1.

As a kind of high-order Gaussian beams, the spot radius and far-field divergence angle of Laguerre-Gaussian beams are related to the

fundamental mode Gaussian beams [29]. The spot radius of Laguerre-Gaussian beams is defined as the distance between the point where the field amplitude falls to $1/e$ of the outermost maximum and the center of the beam [30]. In general, the single ring Laguerre-Gaussian beam is the OAM beam with the simplest optical field structure, and it has higher application value [31].

When the radial exponent of Laguerre-Gaussian beam is equal to 0 and $l \neq 0$, the LG beam is also called TEM_{01} beam, also known as annular beam [32–34]. It is one of the most classical and easy to produce diffusive hollow beam. The hollow TEM_{01} beam, whose the intensity distribution is trapezoidal, has divergence and a dark hollow region in three-dimensional space. Because it has the same orbital angular momentum as the vortex beam, it is also a kind of OAM beam.

2.2. Bessel beams

Bessel beams are non-diffracted beams, which are special solution of Helmholtz equation in cylindrical coordinate [35–37]. Similar to the Laguerre-Gaussian beams, the non-zero-order Bessel beams are also OAM beams with helical phase structure [38], [39], and each photon they contains carries OAM. Fig. 2 shows the simulation results of field intensity and phase distribution of different Bessel beams. The complex amplitude distribution of the l order Bessel beam is [40]

$$BS_l(r, \varphi, z) = A_l J_l(k_r r) \exp(ik_z z) \exp(il\varphi) \quad (4)$$

Where, A_l is a constant, k_r and k_z are wave numbers in the radial direction and beam propagation direction respectively, and they are satisfied with the wavenumber k :

$$k_r^2 + k_z^2 = k^2 = \frac{4\pi^2}{\lambda^2} \quad (5)$$

If there is an obstacle in Bessel beams' propagation path, the light field can recover itself after passing through the obstacle at a certain distance, that is, Bessel beams have self-healing property [41], as shown in Fig. 3. When there is an obstacle in the propagation path of the Bessel beams, the unblocked light will re-interfere behind the obstacle and form the Bessel beams again to realize the self-healing of the light field [35,42]. In addition, the generalized helical Bessel beam was generated by the curved fork hologram [43]. The experimental results showed that any order of generalized helical Bessel beam can be created by illuminating the curved fork hologram by Laguerre-Gaussian beam.

2.3. Bessel-Gaussian beams

Because the Bessel beams have infinitely extended light field structure, they are only ideal theoretical models and cannot really exist. In practice, the Bessel-Gaussian beams are generally used as the approximation of the Bessel beams [44]. The Bessel-Gaussian beams have the non-diffraction characteristic similar to that of the Bessel beams in the finite propagation distance. When beyond the maximum propagation distance, the Bessel-Gaussian beams will no longer exist [45,46]. The complex amplitude of l order Bessel-Gaussian beams can be expressed as

$$BG_l(r, \varphi, z) = A_l J_l(k_r r) \exp(ik_z z) \exp(il\varphi) \exp\left(-\frac{r^2}{\omega_0^2}\right) \quad (6)$$

In the formula, ω_0 is the limited aperture size and z represents the propagation direction of the beam. Formula (6) holds only at the initial light source plane ($z = 0$). When the off-axis Bessel-Gaussian beam propagates for a certain distance, according to the Fresnel diffraction integral formula, the expression of the light field at the observation surface (the plane after the propagation distance z) is [47–49]

$$E(x, y, z) = \frac{1}{i\lambda z} \exp(ikz) \iint E(x_0, y_0, 0) \exp\left[\frac{ik}{2x} (x - x_0)^2 + \frac{ik}{2x} (y - y_0)^2\right] dx_0 dy_0 \quad (7)$$

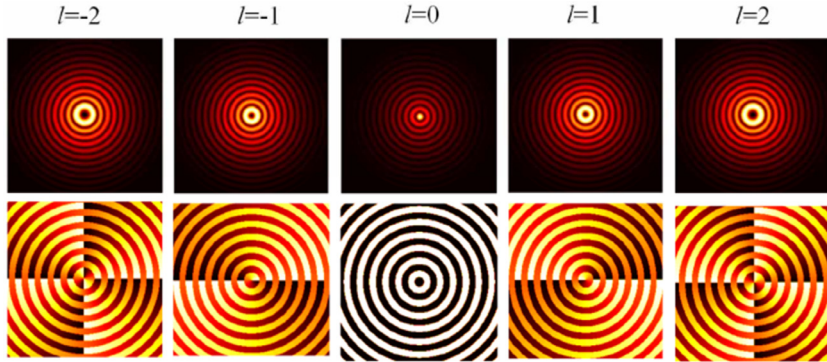


Fig. 2. The simulation results of field intensity and phase distribution of different Bessel beams [31].

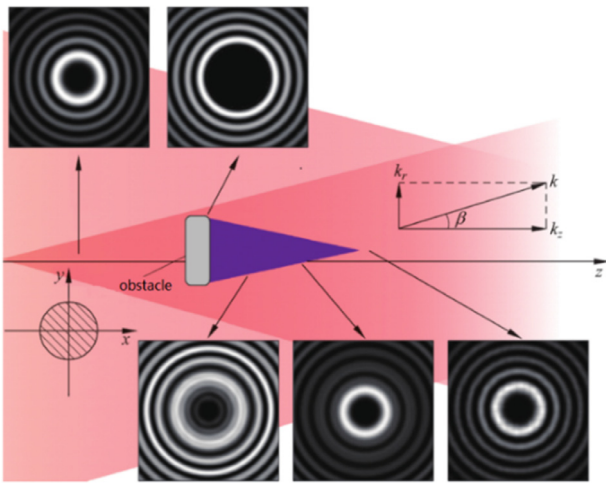


Fig. 3. The self-healing property of Bessel beams [26].

It can be seen that compared with the expression of complex amplitude of the Bessel beams, this expression only has more real term $\exp(-\frac{r^2}{\omega_0^2})$ than the ideal Bessel beams, indicating that the Bessel-Gaussian beams have the same phase structure as the ideal Bessel beams. When $l \neq 0$, each photon contained in the Bessel-Gaussian beams carries OAM. Fig. 4 shows the light field distribution of different orders of Bessel-Gaussian beams. The intensity of the Bessel-Gaussian beams can be obtained from the complex amplitude of them:

$$I_{BG} = |BG_l|^2 \propto J_l^2(k_r r) \exp\left(-\frac{2r^2}{\omega_0^2}\right) \quad (8)$$

For a beam of Bessel-Gaussian beams, both k_r and ω_0 are fixed values.

Bessel-Gaussian beams only exist in limited propagation distance, which is different from the existence of Bessel beams in the whole space. The reasons for these differences can be explained by the interference field [50–52]. The Bessel beams are superimposed by many plane wavelets with equal amplitude and the direction of the wave vector is at β angle to the optical axis. The wavefronts of these plane wavelets continue infinitely and have no aperture. For Bessel-Gaussian beams, although these plane wavelets are also superimposed by these plane wavelets, these plane wavelets have aperture limitations and do not have an infinitely extended wave surface. This makes the Bessel-Gaussian light field range related to the aperture size and diffraction angle β [53,54].

2.4. Hermite-Gaussian beams

Hermite-Gaussian beams, like Laguerre-Gaussian beams, are paraxial approximate solutions of the Helmholtz equation. Therefore, the

Laguerre-Gaussian beam can also be obtained by superposing the Hermite-Gaussian beam [55,56]. However, the Hermite-Gaussian beam is the paraxial approximate solution of the Helmholtz equation in the Cartesian coordinate system, and the Laguerre-Gaussian beam is the approximate solution in the cylindrical coordinate system. The intensity distribution of Hermite-Gaussian beam shows a petaloid structure. Under the experimental conditions, it can be realized by a gradient phase mirror and a fiber coupled laser [57]. The light field expression of the Hermite-Gaussian beam in the propagation direction(z axis) is as follows:

$$E_{uv}(x, y, z) = A_{uv} \frac{\omega_0}{w(z)} H_u \left[\frac{\sqrt{2}x}{w(z)} \right] H_v \left[\frac{\sqrt{2}y}{w(z)} \right] \exp \left[-\frac{x^2 + y^2}{w^2(z)} \right] \exp \left[ikz + i \frac{k(x^2 + y^2)}{2R(z)} \right] - (u + v + 1)\theta(z) \quad (9)$$

Where $H_m(\cdot)$ is the m-order Hermit polynomial, A is the normalization factor, ω_0 is the beam waist radius, and $w(z) = [2(z^2 + z_R^2)/(kz_R)]^{1/2}$ is the beam width at the distance from the beam waist to z .

In addition to the above Hermite-Gaussian beams, an elliptical vortex Hermite-Gaussian beam was reported [58]. Its orbital angular momentum depends on the parameters of the Gaussian beam and ellipticity parameters. The elliptical vortex Hermite-Gaussian beam is formed by the superposition of $n + 1$ generalized Hermite-Gaussian beams, and the complex amplitude is proportional to the n-order Hermite polynomial.

2.5. Perfect vortex beams

When the waist of the fundamental mode is fixed, the cross-sectional spot diameter of the OAM beam is related to the angular quantum number. The larger the absolute value of the angular quantum number, the larger the spot diameter and the larger the hollow region. This characteristic of OAM beam makes it very limited in some applications. For example, in the technology of particle capture and manipulation, the larger angular quantum number and smaller spot diameter are often needed at the same time to achieve a better capture effect. The perfect vortex beam can solve above problems [59–61]. The diameter of the cross-sectional spot is independent of the angular quantum number and can be controlled by multiple parameters [62]. For different order perfect vortex beams converted from the same Gaussian beam through the same system, their spot diameters are all the same.

The ideal perfect vortex beam is a kind of OAM beam whose spot diameter is independent of the angular quantum number. Its ring width approaches zero while the power density on the ring approaches to infinity. The perfect vortex beam can be expressed as:

$$POV_l(\gamma, \varphi) \equiv \delta(r - r_0) \exp(il\varphi) \quad (10)$$

In the formula, r_0 is the spot radius of the perfect vortex beam, l is the angular quantum number, and $\delta(\zeta)$ is the Dirac function.

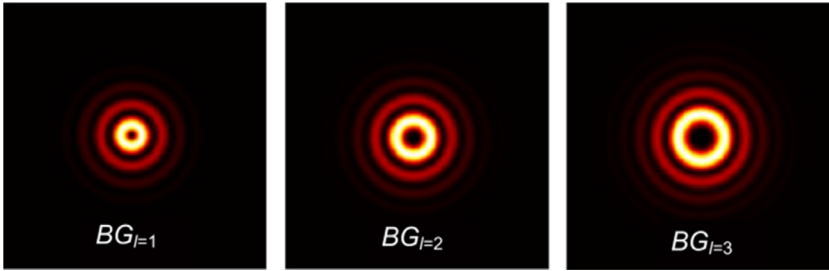


Fig. 4. The light field distribution of different orders of Bessel-Gaussian beams [38].

2.6. Some novel OAM beams

In the cylindrical coordinate system, in addition to the solutions of Bessel and Laguerre-Gaussian modes, the solution of the Schrodinger equation can be regarded as a degenerate hypergeometric function, which is called Hypergeometric mode [63]. The intensity distribution on the cross section of Hypergeometric mode is similar to that of the Bessel mode, which is a group of concentric rings. And the Hypergeometric beam has many similar characteristics to the Bessel beam [64,65]. However, unlike the Bessel mode, the ring radius of the Hypergeometric mode increases with the increase of the ordinate z . In the experiment, diffractive optical elements and computer-generated holograms are generally used to generate this kind of laser mode [65,66], which can be used in laser processing.

Beams with self-focusing characteristics, such as generalized Airy beams, circular Airy beams, Pearcey beams, circular Pearcey beams, aberration beams, radially sublinear and superlinearly chirped beams, have received great attention [18,67–70]. It was proposed that the vortex beam with self-focusing characteristic can be shaped by spatial light modulator, and the resulting light field could be used in the field of laser manipulation and laser material processing [71]. The combination of vortex beam and Airy beam, that is, the Airy vortex beam with optical vortex, especially the circular Airy vortex beam, is an interesting, hot and potential research content with wide application potential [72–78]. Airy vortex beams and circular Airy vortex beams have application prospects in studying the conversion of OAM and spin angular momentum, regulating the self-focusing properties of light field, optical communication and particle manipulation. Propagation properties and potential applications of this kind of beam are of research significance, so it is still a research hotspot. A technique was proposed to generate multiple circular Airy Gaussian vortex beams with independent topological charges and initial emission angles by a single digital hologram encoded on a spatial light modulator [79]. This technology paves the way for simultaneous manipulation of particles in three-dimensional space, and provides another way to realize optical communication in multi-spatial optical modes.

Pearcey beam is the generalized form of Bessel beam. It is a kind of self-repairing beam similar to Airy beam, which has additional auto-focusing properties during propagation [80–83]. Pearcey Gaussian vortex beam(PGV) maintains the self-focusing, self-healing and shape invariance of Pearcey beam and Pearcey Guassian beam. Due to the influence of optical vortex, a bright spot appears in front of the main lobe of PGVB, which makes it have the most significant intensity singularity and phase singularity. Moreover, in Kerr medium, the auto-focusing ability of PGVB increases with the increase of power, and still has the characteristics of self-focusing, self-healing and shape invariance [84].

In summary, with the in-depth study of OAM, more and more kinds of beams with helical phase are proposed. In recent years, in addition to the above-mentioned OAM beams, some vortex beams with multi-vortex arrays [85–88], fractional OAM[89–93] and special profiles [81,82,94] have aroused great interest in the development of new theories and technologies. The study of the novel structural vortex light field is of great significance to the cutting-edge scientific research.

3. Generation technology of OAM beams

The generation of OAM beams is the important basis for the study of their properties and applications. Since the angular quantum number l is the eigenvalue of the OAM beams, it determines the amount of OAM carried by each photon in the OAM beams, which indicates the purpose of generating the OAM beams is to obtain the OAM beams of any order. With the in-depth study of OAM, more and more OAM beams generation methods have been proposed. The generation technology of OAM beams can be divided into two categories: intra-cavity mode selection method and extra-cavity conversion method. The intra-cavity mode selection method generates OAM beams directly in the laser resonator, while the extra-cavity conversion method converts other forms of beams, such as Gaussian beams and Hermite-Gaussian beams, into OAM beams. In this chapter, the intracavity method and the extra-cavity conversion method, which are used to generate OAM beams, are introduced in detail.

3.1. Intracavitory method

The intracavity method generates the OAM beams in the resonant cavity. This method is the first method to generate vortex light with spiral wavefront, and it is of great significance for researchers to study OAM later. In this section, the intracavity mode selection method and digital laser are introduced to generate OAM beams in detail.

3.1.1. Intracavity mode selection

The intracavity mode selection method [95] is to realize the selection of Laguerre-Gaussian beams by adding loss in the laser resonator. Tamm first reported the method of obtaining Laguerre-Gaussian modes directly from laser resonators in 1988 and 1990 [96,97]. By introducing the loss of low-order modes into the laser resonators, the generation of fundamental modes is suppressed and higher-order transverse modes are generated more easily, thus the required Laguerre-Gaussian beams are obtained. However, because of the high loss, this method is not easy to generate OAM beams with large topological charge, and it is not easy to output high power OAM beams [98].

Changing the spot shape of the pump light can realize the output of high-order modes, which is also a method of mode selection in the cavity. In the case of annular pump light, Kim proposed a mode selection etalon placed at a specified angle in the resonant cavity, as shown in Fig. 5, which destroys the helical propagation symmetry of two opposite Laguerre-Gaussian beams with the helical wavefront, leads to the selection of the wavefront rotation direction and makes one mode oscillate while suppressing the other mode, thus obtaining the superposition state [99]. Compared with the method of suppressing the fundamental mode oscillation in the resonant cavity, this method is more efficient. Its simplicity and robustness will be conducive to the development of a series of new laser systems with optical vortex output [100]. However, in order to output other order OAM modes, it is necessary to change the shape of the pump light and adjust the placement angle of the mode selection etalon, which greatly reduces the flexibility of generating different order OAM beams.

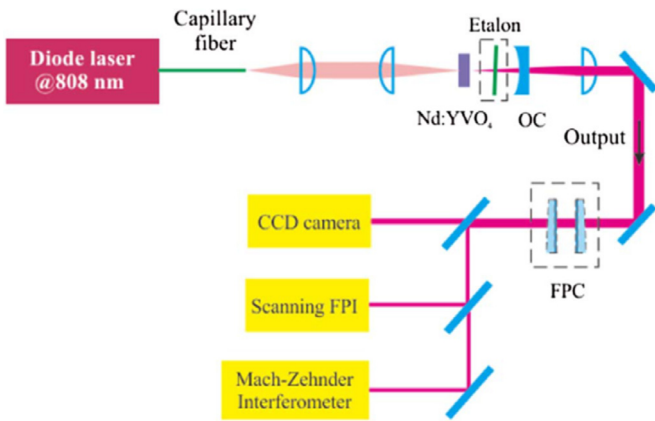


Fig. 5. The experimental device for introducing a mode selection etalon in the resonant cavity [46].

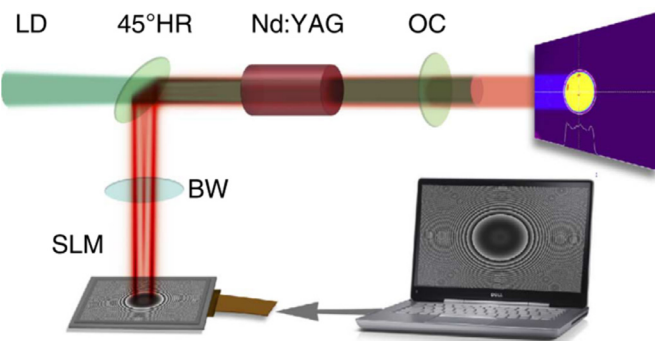


Fig. 6. The working principle diagram of the proposed digital laser [51].

3.1.2. Digital laser

Traditional lasers can only generate a single laser mode without changing the resonant cavity parameters. In recent years, in order to meet the demand of arbitrary laser mode output without changing the resonant cavity structure, the digital laser was proposed. This equipment can real-time select any laser mode for output [101], which is undoubtedly of great significance to the output of OAM modes.

The digital laser was first proposed by Ngcobo [102]. Its principle is to use a reflective liquid crystal spatial light modulator instead of a mirror in the traditional laser resonator, and the spatial light modulator and another mirror form laser resonator to realize laser output. By changing the modulation pattern loaded into the spatial light modulator, the laser can achieve a variety of OAM beams with different orders output. Fig. 6 shows the working principle diagram of the proposed digital laser.

Digital laser can obtain any laser mode without changing the laser resonator, and can be widely used in real-time control of thermal lens, mode control and switching between aberration and real-time [103]. However, there are still some problems. The reflectivity of liquid crystal spatial light modulators is generally not high. Under current technical conditions, the reflectivity of liquid crystal spatial light modulators is 60% ~ 90% [104], which makes the loss in the resonant cavity very large, and many laser modes are not easy to start up. In addition, because the damage threshold of liquid crystal spatial light modulator is low, spatial light modulators are easy to be damaged if the power of incident light is large. Therefore, it is not suitable for digital laser to obtain high power laser output, and the conversion efficiency is very low [105].

In summary, with the further study of the generation method of OAM beams, it is found that there are many problems of OAM beams generation in intracavity. At present, when the intracavity method is used to generate OAM beams, there are some problems that the order cannot be adjusted, or the order can be adjusted with low efficiency. Therefore, in

the application of vortex beams, the out-of-cavity conversion method is often used to generate OAM beams with different orders.

3.2. Extracavity conversion method

The out-of-cavity conversion method means that outside the resonator, other forms of beams, such as Gaussian beams and Hermite-Gaussian beams, are converted into OAM beams by certain technical means. Because the generation of OAM beams by extracavity conversion method avoids the deficiency of intracavity method in generating OAM beams to some extent, more and more researchers are interested in converting other beams into beams with OAM, and an increasing number of techniques for generating OAM beams by extracavity method have been proposed. In this section, mode converter, helical phase plate, fork grating, phase type diffraction vortex grating and metasurface are introduced to generate OAM beams outside the cavity.

3.2.1. Mode converter

The mode converter is composed of several cylindrical lenses placed in a certain relationship, which can convert high-order Hermite-Gaussian beams into high-order Laguerre-Gaussian beams [106–108]. In 1991, the integral transformation from Hermite-Gaussian beam to Laguerre-Gaussian beam was proposed for the first time by Abramochkin. He verified it with cylindrical lens experimentally. Furthermore, the integral search process was given in detail in the appendix [109]. Fig. 7 shows a mode converter [110] composed of two cylindrical lenses with the same optical axis direction. The mode converter can be divided into $\pi/2$ converter and π converter according to the distance of the lens. The $\pi/2$ converter can cause the phase difference between the adjacent low-order Hermite-Gaussian beams components of the incident Hermite-Gaussian beams HG_{mn} , and then convert the incident beams into LG_{pl} mode, which satisfies $p = \min(m, n)$, $l = m - n$. Since $m, n \geq 0$, in order to obtain single-ring Laguerre-Gaussian beams, the order m or n of the incident Hermite-Gaussian beams must be zero. For the π converter, the phase difference introduced to the adjacent low-order Hermite-Gaussian components is π , so the incident HG_{mn} or LG_{pl} can be converted into their respective mirror modes HG_{mn} or LG_{p-l} . What should be noted is that the function of these cylindrical lens converters is mathematically similar to the polarization of birefringent $\lambda/4$ and $\lambda/2$ plates, respectively. The difference is that the wave plate manipulates the spin angular momentum of the photons, while the mode converter manipulates the OAM of the photons [111]. When the higher-order Hermite-Gaussian modes pass through the mode converter, the low-order relative phase will change, and when the relative phase change satisfies a certain relationship, a specific order Laguerre-Gaussian beam can be obtained, as shown in Fig. 8. In addition, Gao proposed a mode converter composed of three cylindrical lenses placed in different directions [112], which can convert the incident HG_{m0} mode into an OAM beam with angular quantum value of $-m$, which provides a solution for outputting OAM beams through cylindrical lens in the future.

In summary, in an ideal condition, the mode converter can completely convert the incident Hermite-Gaussian beams into OAM beams. And its conversion efficiency is very high, so it has great potential application value in the manipulation of particles [19,113,114] and rotation body detection [115]. However, the mode converter still has some limitations. First of all, a specific order Hermite-Gaussian beam needs to be generated by certain technical means. Secondly, the volume of the mode converter is large, which has strict requirements on the relative position and angle of the cylindrical lens.

3.2.2. Spiral phase plate

The characteristic of OAM beams is that they have spiral wavefront. If the plane wavefront of Gaussian beams is directly transformed into spiral wavefront by certain means, OAM beams can be obtained [116]. The plane wave can be converted into OAM beams by introducing spiral wavefront with spiral phase plate, which is the most direct method to

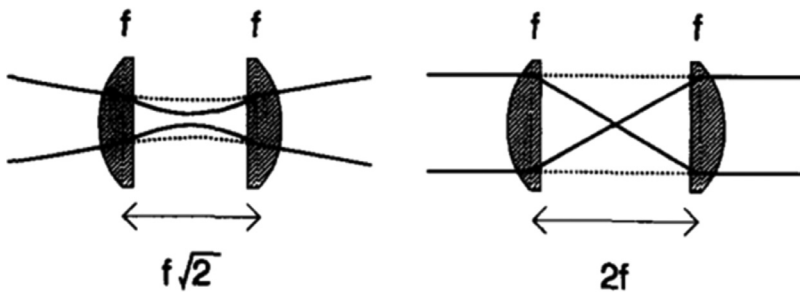


Fig. 7. The mode converter consisting of two cylindrical lenses [56].

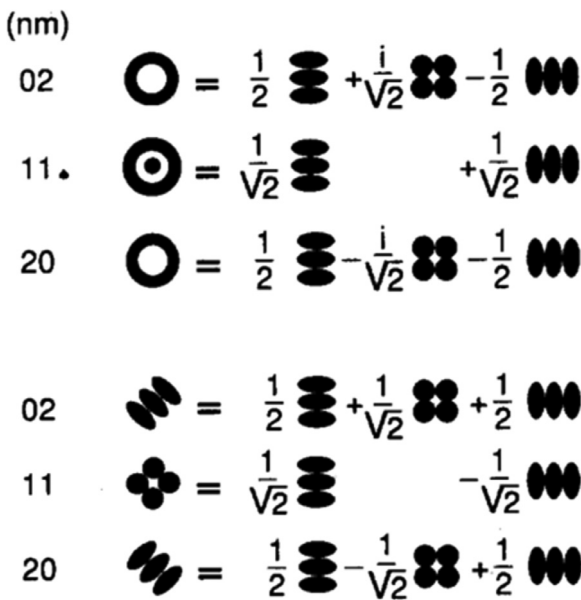


Fig. 8. Both the Hermite-Gaussian modes and the Laguerre-Gaussian modes can be decomposed into the superposition of different lower order Hermite-Gaussian components [56].



Fig. 9. The complete modular physical diagram of the designed spiral phase board [63].

generate OAM beams. In 1992, the filter with phase spiral distribution, namely spiral phase plate, was proposed for the first time [117]. The experimental results showed that the coherent light could be focused on a narrow ring by coupling the spiral phase plate with biaxial prism and spherical lens, which lays a foundation for the generation of vortex beams through the spiral phase plate in the future. Later on, Peter successfully generated a micron wavelength OAM beam by using the designed modular spiral phase plate [118], as shown in Fig. 9. Besides,

through formula derivation and experiments, Kotlyar verified that the inaccurate alignment of the designed spiral phase plate center and intensity distribution center of light ring could not affect the total OAM of the beams [119], which provides a reference for the future study of the special design of spiral phase plate to generate OAM beams. Because the method of generating OAM beams by spiral phase plate is very direct, it has wide application space in the field of communication [118,120,121].

Although the study of spiral phase plate to output OAM modes has been favored by many scholars, in order to make the output purity of vortex beam higher, the surface of spiral phase plate must be very smooth. Meanwhile, the thickness distribution of the spiral phase plate must strictly satisfy the expression of the relation between phase and optical path [118,122,123]. In addition, the spiral phase plate is generally only aimed at the vortex beam of a specific wave band, and different spiral phase plates need to be made for different wavelengths of incident light, which increases the fabrication technology and the cost of the spiral phase plate [124] and undoubtedly increases the limitation of its wide application.

3.2.3. Forked grating

Forked grating is a kind of grating with forked structure. The generation of vortex beams with fork gratings was first proposed by Bazhenov [125]. In the experiment, diffraction to the laser beam was achieved by a forked grating synthesized with computer. The experimental observation demonstrated that in the far field diffraction region, there was spiral wave of zero intensity at ± 1 diffraction grade of the grating. And the existence of beams with spiral wavefront was experimentally demonstrated as well. When Gaussian beam passes through a forked grating, a vortex beam with OAM appears at the ± 1 diffraction order of the far-field diffraction, and the order of the OAM beam is related to the number of grating forks. When using the forked grating to generate the OAM beams, only the beam at the ± 1 diffraction order is considered. And the order of the OAM beams at the ± 1 diffraction order is determined by reasonably selecting the number of intermediate forks [126]. In practical applications, -1 or $+1$ order diffraction is usually used to obtain purer OAM beams. In this case, the ideal conversion efficiency of Gaussian beams to OAM beams is only 10.13% [127]. Although the efficiency of generating OAM beams by forked grating is not high, this method has become one of the main means to generate OAM beams because of its easy fabrication and low cost.

In addition to being used to generate OAM mode, the research of forked grating for OAM mode conversion has also been reported. That is, through the design of the fork grating, the OAM mode generator as well as an efficient conversion of the OAM modes which can be controlled by polarization is realized, and the conversion efficiency is as high as 100%. Based on the above analysis, it is proposed that one can consider using the fork grating instead of the spiral phase plate to generate OAM beams [128]. Recently, a similar design has been proposed, showing an integrated device that emits beams carrying superimposed OAM modes by embedding superimposed angular gratings in a WGM microring resonator [129]. The experimental device is shown in Fig. 10. Thus it can be seen that because of the competitive advantages of simple

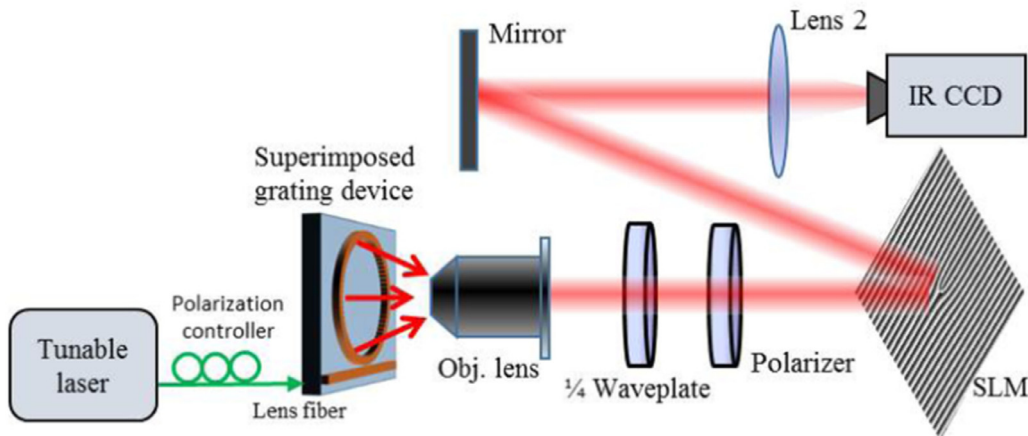


Fig. 10. Experimental device diagram for generating superimposed OAM beams [73].

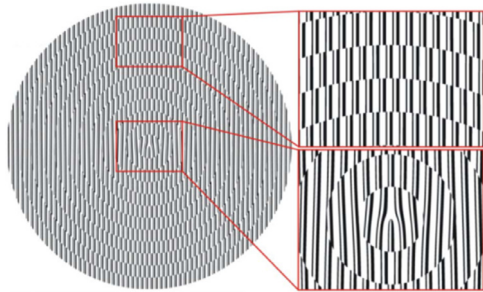


Fig. 11. The designed composite Dammann vortex grating [79].

processing, small size and light weight, the method of generating OAM modes by forked grating may greatly promote the wide application of OAM modes, and can be used in the field of measurement to realize the detection of rotating objects [130–132].

3.2.4. Phase diffractive vortex grating

Phase diffractive vortex grating is a kind of optical device which generates OAM beams by phase modulation of incident Gaussian beams. Compared with amplitude grating (such as forked grating) [133], the diffraction efficiency of phase vortex grating is greatly improved. However, the fabrication process of phase diffractive vortex grating is complicated and the production cost is high, so it has not been widely used. The appearance of liquid crystal spatial light modulator makes it possible to use electrical signal coding to control liquid crystal molecular deflection to realize the simulation of phase diffractive vortex grating [134], which promotes the application of phase vortex grating to some extent.

The method of using programmable spatial light modulator and Dammann grating to generate OAM beams has been welcomed by many researchers. Yu proposed a new type of diffractive optical element – composite Dammann vortex grating (CDVG) [135], as shown in Fig. 11, which can produce a controllable petal-shaped OAM mode with the purity of up to 90%. And the petal pattern is rotated continuously by the programmable spatial light modulator dynamically changing the relative lateral displacement, which provides the possibility to quantitatively control the rotation speed of the optical clamp. And this method has great potential application value in the field of optical manipulation. In the same year, Lei reported the design of a large number of OAM channel multiplexing through Dammann vortex gratings [136]. Fig. 12 shows communication schematic diagram of free-space optical multiplexing/demultiplexing based on OAM using the designed grating. Multiplexing of 10 OAM states, 80 wavelengths and two polarizations

is realized on 1600 separately modulated orthogonal phase shift keying (QPSK)/16-QAM data channels, and the 80/160 Tbit/s capacity and uniform power distribution are realized on all channels, which makes it possible to increase the capacity of optical communication system to the Pbit/s level. In recent years, beyond that, researchers pay more and more attention to the special design of phase grating to realize the output of OAM modes. Some scholars proposed a scheme of using the plasma grating to obtain tilted OAM beams [137]. Subsequently, a high-order spiral long-period fiber grating which could generate both second-order and third-order OAM modes was reported, and its conversion efficiency was more than 95% [138].

The method of using liquid crystal spatial light modulator to simulate vortex grating to generate OAM beams is very flexible [139] and the holographic phase loaded can be changed according to the need. However, when the order of the vortex grating is very large, the central phase jump of the vortex grating is very high. Because the resolution of the spatial light modulator is limited, the simulation of the high-order phase vortex grating is insufficient. This lack of central resolution will lead to the widening of the band of the generated spiral beams. The problem that the high-order vortex beams generated by the high-order vortex grating is not ideal can be solved by the optimal ring method [140,141]. The method of generating OAM beams by phase vortex grating has great potential application value in the field of optical manipulation [142], and when this method is combined with space division multiplexing, it is of great help to solve the crisis of communication capacity.

3.2.5. Metasurface

Most of the traditional OAM beams generation methods are based on standard optical equipment, such as spiral phase plate and spatial light modulator [143,144], which are suitable for laboratory experiments, but there are some problems, such as material thickness, large volume, long working distance and relatively low optical control precision, which may be incompatible with integrated optical systems and the optical systems that require ultra-miniature and flat plate optics. In recent years, the realization of micro-size planar optical elements based on metasurface has become possible. Ultra-compact, low-loss, fast and reconfigurable optical elements can manipulate light on a nanometer scale. The hypersurface of nanostructures has been proved to be able to effectively control the amplitude and phase of light in the linear optical region, and the wavefront of the beams can be reconstructed, thus introducing OAM into the beams [145,146].

Hypersurface is a kind of structured interface with different nanostructure contours, which is developing rapidly. The hypersurface can cause a sudden phase change for the incident light wave through a retractable artificial atom, thus a beam carrying OAM can be obtained

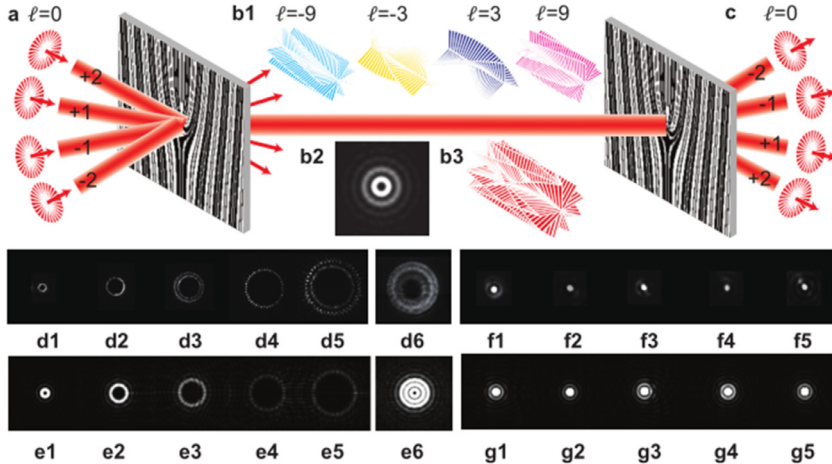


Fig. 12. Communication schematic diagram of free-space optical multiplexing / demultiplexing based on OAM using the designed grating [80].

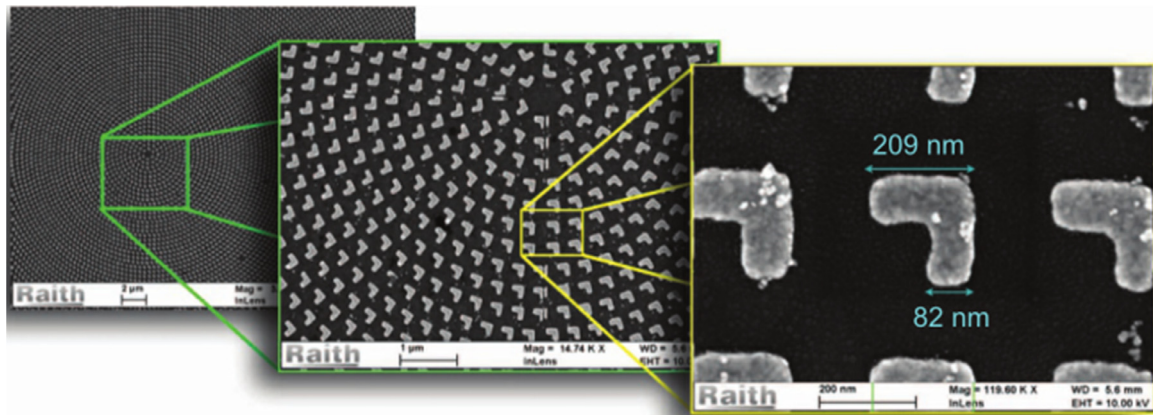


Fig. 13. The schematic diagram of the proposed plasma nanostructure [93].

[147]. Different polarization effects can be transferred to the orbit through the interaction between spin angular momentum and OAM, opening up new application value in manipulating orbits [148]. As shown in Fig. 13, it was proposed to convert circularly polarized light into light with OAM by birefringence of plasma nanostructures [149], which provides a strong support for the application of OAM beams in the field of medical diagnosis. However, most of the plasma hypersurface designs have the problem of low coupling efficiency, and because it is based on metal resonators, it will lead to ohmic loss. Based on the above problems, a method to replace the plasma hypersurface was proposed, that is, the high refractive index silicon cutting line combined with silver layer is used to replace the metal resonator. The use of dielectric resonators instead of plasma resonators can pave the way for ultra-efficient high-frequency subsurface devices [150]. So far, researchers have realized the reconstruction or tuning of optical properties through the all-dielectric hypersurface. However, most of the proposed tuning methods either require high optical power or low efficiency [151]. The hypersurface based on As_2S_3 sulfide glass can overcome the above problems. It can reshape the traditional Hermitian-Gaussian beams without OAM into OAM beams at low intensity, while maintaining the amplitude and phase characteristics of the original beams at high intensity. The technology of designed hypersurface to generate OAM beams can be applied in ultra-high speed compact optical communication system, optical signal processing and all-optical switching [152]. In addition to generating OAM beams, the researchers also proposed some hypersurface structures with additional functions, such as eliminating chromatic aberration response, detecting and demultiplexing OAM beams [153], etc., which are of great significance to the application of OAM beams in the field of communication. However, the above methods of

generating OAM beams through the hypersurface are all based on the reflected hypersurface and are not compact enough because of the existence of the air layer. [154] improved the structure of the hypersurface and proposed a transmission hypersurface, which was designed to generate dual-mode and dual-polarized OAM beams at the same time, which provides another effective solution for generating OAM beams from the hypersurface.

In addition to the above schemes, the application of anisotropic crystal in the conversion of spin angular momentum to OAM can be used to realize the conversion of OAM beam, and the plasmon can be used to generate OAM beam as well. In uniaxial crystals, Bessel beams can be converted into other OAM beams by means of spin-to-orbital angular momentum conversion. Note that for Gaussian beams, the maximum of conversion efficiency is 0.5, but for high-order elegant Hermite-Gaussian beams and Laguerre-Gaussian beams, the conversion efficiency can be increased to 0.9. For Bessel beams, the efficiency can be close to 1 [184,185]. Therefore, the use of uniaxial crystals is also an effective means to generate OAM beams. In addition, the plasma vortex lens can couple the spin angular momentum and orbital angular momentum into the plasma vortex, that is, the OAM beam is generated. On this basis, the plasma generator can be used to generate and detect OAM at the same time [166].

All above are techniques for generating OAM beams with helical wavefronts in free space. In addition, the OAM beams can also be generated based on the optical fiber integrated link [186,187]. The technology of generating OAM beams from optical fiber can be divided into three types: optical waveguide device conversion method [188], optical fiber coupling conversion method [171–176] and photonic crystal fiber (PCF) conversion method [177–183]. The scheme of directly generat-

Table 1
Performance comparison of difference schemes of generating OAM beams.

Generation method	Cost	Conversion efficiency	OAM mode	Processing difficulty	System complexity	Reference
Intracavity mode selection	High	Low	Single	Low	High	[96],[97],[99],[155],[156]
Digital laser Mode conversion	High	Low	Single	Low	High	[101],[105]
SPP	Low	Normal	Single	High	Low	[118],[119],[121],[157]
Fork grating	Low	Low	Single	Low	Low	[128],[129],[158–160]
Phase vortex grating	High	High	Single/multiple	High	Low	[134–139],[161]
Metasurface	Low	Relatively high	Single	High	Low	[138–147]
Uniaxial crystal	Normal	High	Single	High	Low	[162–165]
Plasma generator	High	High	Single	High	Low	[166–170]
Optical fiber integration	Normal	High	Single/multiple	High	Low	[171–176]
PCF	Normal	High	Single/multiple	High	Low	[177–183]

ing OAM beams in the optical fiber simplifies the optical system, and the OAM beams are obtained by the superposition of the corresponding order vector modes in the optical fiber, and their phase purity is higher. The comparison of multiple performance parameters of different schemes for generating OAM beams is shown in Table 1.

4. Application of OAM beams

As a new type of laser beams, OAM beams have very important application value in many fields. For example, because different OAM modes are orthogonal to each other, OAM beams can be used to expand the channel capacity of optical communication systems, and the rotating Doppler effect of vortex beams can be used to detect rotating bodies including motors, rotating fluids, atmospheric vortices and so on. In addition, the OAM beams have the characteristic of OAM, so they can also be used in the fields of particle manipulation, celestial body detection, etc. In this chapter, the applications of OAM beams in ultra-large capacity optical communication, rotating object detection, optical tweezers, laser processing and super resolution imaging are introduced.

4.1. Ultra-large capacity optical communication

With the arrival of the era of cloud computing and big data, the demand for the bandwidth capacity of optical communication is also increasing. In the past few decades, the multiplexing technology of optical amplitude, phase, wavelength and polarization has increased the data carrying capacity of optical communication systems by four orders of magnitude, but the data transmission capacity of single-mode optical fiber is close to Shannon's limit. It is difficult to use the above dimensions of light to further enhance the communication capacity [5]. In recent years, with the in-depth exploration of OAM beams, it is found that OAM can be multiplexed as a new dimension of photons — OAM mode division multiplexing. In addition, because the angular quantum number carried in the OAM beams can be infinitely large in theory, the coding of OAM states is of great significance to the breakthrough improvement of optical communication capacity. This section will describe the application potential of OAM beams in the field of optical communication from two aspects of OAM mode division multiplexing and OAM coding technology respectively.

4.1.1. OAM beams mode division multiplexing communication

In the optical communication system based on OAM beams, the most promising way is to use OAM beams mode division multiplexing to achieve large capacity information transmission. At the same time, mode

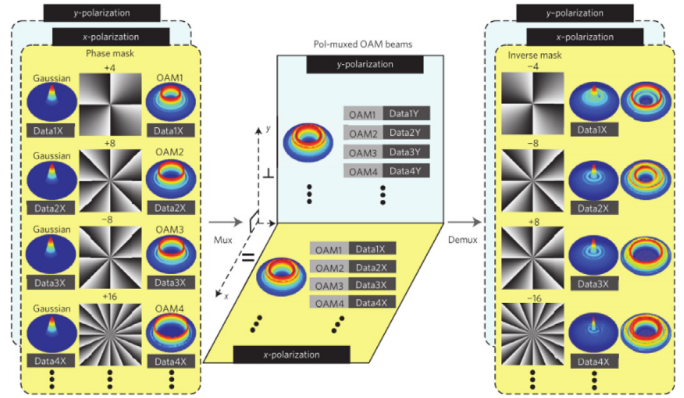


Fig. 14. The principle of communication using different order OAM beams mode division multiplexing combined with polarization multiplexing [190].

division multiplexing can also be shared with other multiplexing methods such as polarization multiplexing and wavelength division multiplexing [189] to further expand the channel capacity on the basis of traditional multiplexing methods, as shown in Fig. 14.

Based on Fig. 14, the process of mode division multiplexing using OAM beams is as follows:

- (1) Different signals are encoded into different fundamental mode Gaussian beams by traditional signal coding methods such as orthogonal phase shift keying;
- (2) The modulated fundamental mode Gaussian beams are converted into different order OAM beams respectively;
- (3) These OAM beams are combined into one beam and participate in other multiplexing modes as a beam.
- (4) The transmitted beam is demultiplexed at the receiving end, and the OAM beams of different orders are separated.
- (5) The transmitted information is obtained by de-multiplexing each OAM beam respectively.

By using the combination of OAM beams mode division multiplexing and polarization multiplexing shown in Fig. 14, the channel capacity can be extended to the order of magnitude of 1 TB/s. If wavelength division multiplexing is introduced on this basis, the channel capacity can be further increased to the order of 100 TB/s. Recently, researchers have achieved 160 TB/s information transmission by simultaneous multiplexing of 10 OAM beams of different orders, 80 wavelengths and 2 polarization dimensions [136].

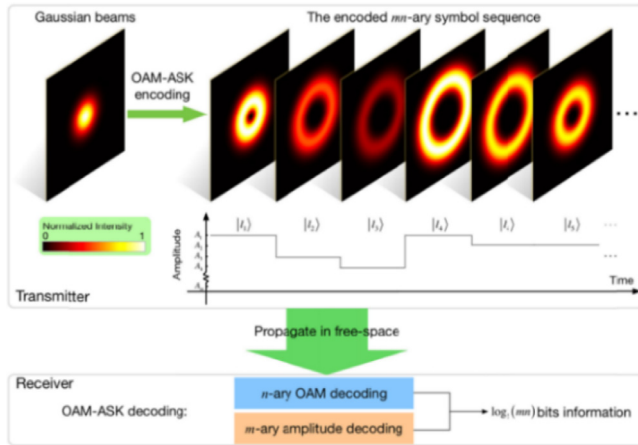


Fig. 15. The schematic diagram of the principle of OAM-ASK [12].

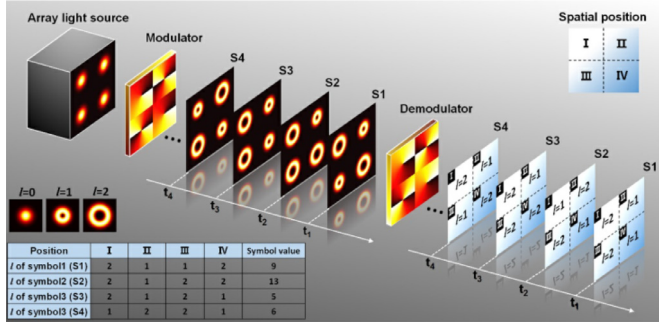


Fig. 16. The schematic diagram of OAM array coding principle ($N = 2, n = 4$ as an example) [12].

4.1.2. OAM coding communication technology

Using the dimension of light to encode the digital signal is an important basis for optical communication. At present, mature digital signal coding methods include amplitude shift keying [191], frequency shift keying [192], phase shift keying [193] and so on. These coding methods make use of the amplitude, frequency and phase dimensions of light respectively. In fact, the OAM dimension of OAM beams can also be used for signal coding, which is called OAM coding technology [6].

In OAM coding technology, because of the diversity of angular quantum numbers of OAM beams (arbitrary integer can be taken), it is theoretically possible to make a code element carry infinite bits of information. OAM coding can also be carried out simultaneously with other optical dimensions, so that the coding efficiency can be further improved in the case of finite OAM states [133]. For example, OAM coding can be combined with ASK technology to encode digital signals, which is called hybrid OAM amplitude shift keying (OAM-ASK) [12] and its principle is shown in Fig. 15. As another example, OAM coding and spatial position coding can be combined to encode digital signals, that is, OAM array coding [11], the principle of which is shown in Fig. 16. In OAM array coding, an OAM array is listed as a code element. Compared with using only OAM coding, the amount of information of each code element is increased by n times, and compared with the traditional binary coding, the coding efficiency is improved by $n \log_2 N$ times.

OAM coding technology makes full use of the OAM dimension of light. Because of the diversity of OAM states, OAM coding can greatly improve the coding efficiency of digital signals. It has a potential application prospect in the future optical interconnection, optical networks and other large-capacity signal transmission.

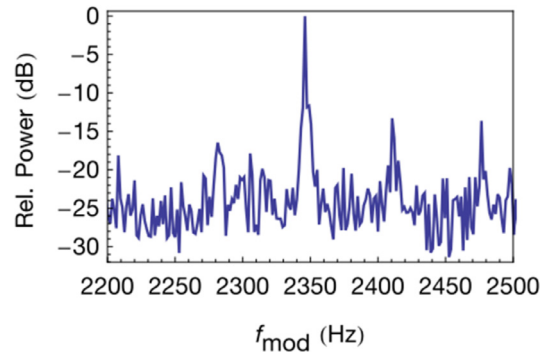


Fig. 17. The frequency domain signal of scattered light measured when ± 18 -order dual-mode hybrid OAM beams irradiates a rotating disk [15].

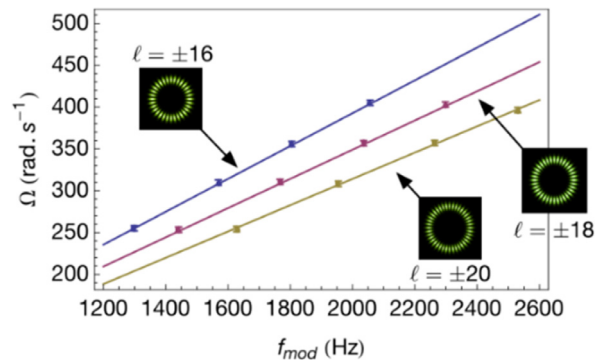


Fig. 18. The relationship between intensity modulation frequency and rotational speed and angular quantum number, in which the real line and scattered point are the theoretical and experimental results respectively [15].

4.2. Rotating body detection

In recent years, it has been found that there is Doppler Effect in rotational motion. When a beam with OAM irradiates on the rotating body along the axis of rotation, the frequency of light will change. This effect is called rotational Doppler Effect [194–196]. Different from the linear Doppler effect, the rotational Doppler effect has the characteristic of achromatic aberration, and the angular velocity of the rotating body can be measured directly by using the rotational Doppler effect [197]. Based on the rotational Doppler effect of OAM beams, this section introduces the application of OAM beams to the detection of rotating objects.

The monochromatic OAM beams in 670 nm band is used to irradiate a rotating metal disk, and the angular velocity of the rotating body is inversely derived by measuring the scattered light signal by a photodetector [14]. Fig. 17 shows the results of the Fourier transform of the signal received by the detector. The angular velocity of the turntable of this time is $\Omega \approx 405$ rad/s. Fig. 18 shows the scattered light intensity modulation frequency measured at different rotational speeds and different orders of incident dual-mode hybrid OAM beams. The frequency spectrum of the detection signal will be amplified when the high-order OAM beams are used for detection, so the detection accuracy can be improved to some extent by using the high-order OAM beams to detect the rotating objects.

Because the frequency shift caused by the rotational Doppler effect is independent of the optical frequency [198,199], it is theoretically feasible to use non-monochromatic light to detect the rotating body. Lavery proposed to use white light (non-monochromatic) OAM beams to measure the angular velocity of the rotating body [15]. The whole measurement system is shown in Fig. 19. The observability of the rotational Doppler shift shows that the rotating sensor formed by the rotational Doppler effect can measure the rotating object remotely even under the

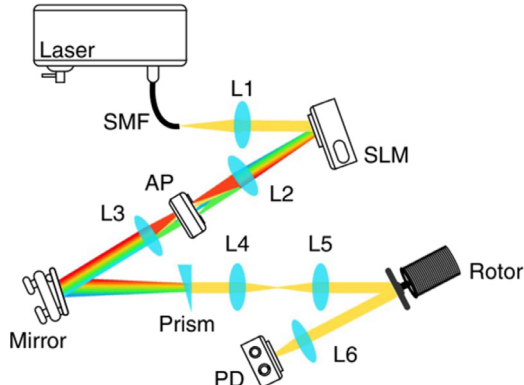


Fig. 19. The experimental system for measuring the angular velocity of a rotating body using white light vortex beams [16].

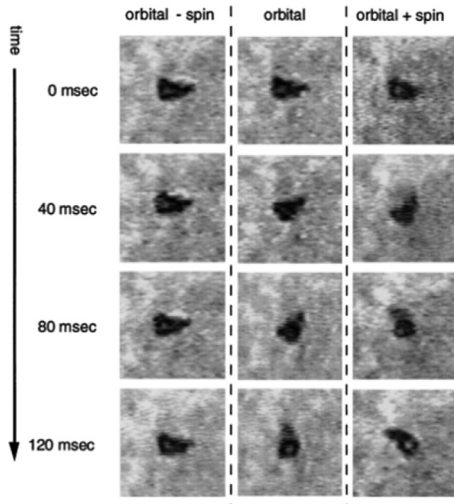


Fig. 20. Rotation of particles caused by OAM and spin angular momentum [135].

white light source. Remote sensing based on this rotational Doppler shift has a broad application prospect in the field of astronomy and land survey [200].

4.3. Optical tweezers

Optical tweezers, also known as beam gradient traps, can be understood as a special light field. When the light field interacts with tiny particles, the whole particles are subjected to the effect of light to achieve the effect of being clamped, thus achieving the purpose of capturing and manipulating them [114,201–203]. The OAM of the OAM beams can be transferred from the optical tweezers to the particles, which makes the particles rotate around the optical axis without any other suspension facilities to form an optical wrench [204]. In this case, the rotation of OAM is realized by the laser absorption of the captured particles.

The annular light field structure of the OAM beams means that the particles can be bound in the region of zero intensity near the optical axis. In order to achieve the axial limitation of the third dimension, the glass sheet can be placed perpendicular to the optical axis. As shown in Fig. 20, + 1-order OAM beams are used to capture and control polystyrene particles suspended in alcohol. Because the particles have partial absorption of the light, the gradient force is sufficient to bind the particles in three-dimensional space and separate them from the container wall [205]. As non-diffracting OAM beams, Bessel-Gaussian beams can also be used in optical tweezers. By using the non-diffraction and self-healing characteristics of zero-order Bessel beams, it is possible to cap-

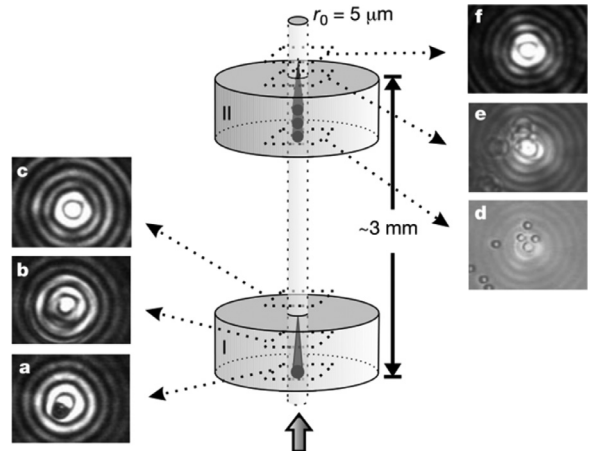


Fig. 21. Capture and manipulate particles longitudinally by Bessel-Gaussian beams [137].

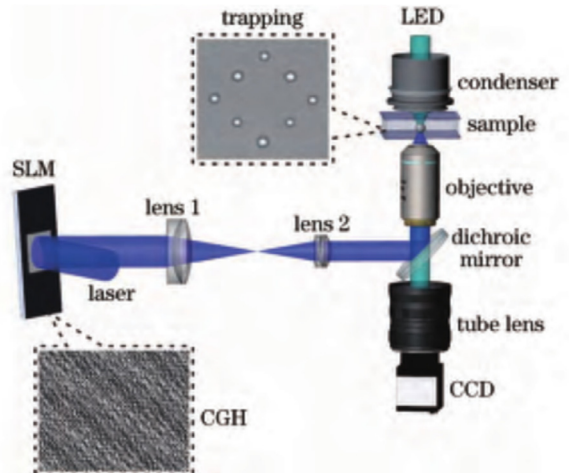


Fig. 22. Holographic optical tweezers system based on liquid crystal spatial light modulator [142].

ture and manipulate multiple particles in multiple planes at the same time, as well as to sort and transport particles [206]. Fig. 21 shows the experimental results of using zero-order Bessel-Gaussian beams to capture and manipulate particles simultaneously in two longitudinally separated 3 mm sample cells [207]. If two-mode coaxial superimposed Bessel-Gaussian beams are used as the manipulating beams, an optical transmission band is formed, which can capture and transport particles up to several hundred microns in length.

With the development of holographic optics and computer technology, the modulation of the target light field and the manipulation of particles can be realized by programming the holographic grating [208,209] loaded on the liquid crystal spatial light modulator. This technology is called holographic optical tweezers [210,211]. Fig. 22 shows a typical holographic optical tweezers system based on liquid crystal spatial light modulator [212]. By reasonably calculating the holographic grating loaded on the liquid crystal spatial light modulator, the OAM beams array is generated to realize the simultaneous capture of multiple particles, and the position and OAM of the OAM beams in the array can be changed by changing the corresponding design parameters to move and manipulate particles captured.

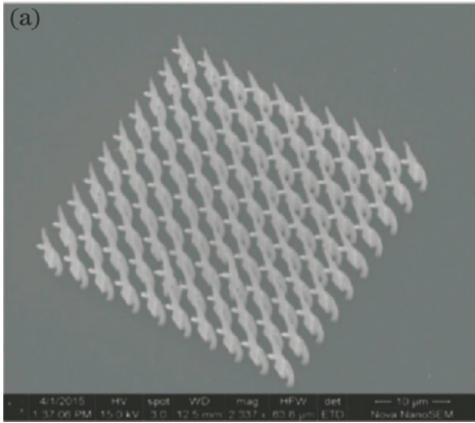


Fig. 23. SEM images of polymerized double-helix microstructures [20]. (a) Double-helix microstructure array; (b)(c) top and side view of a single double-helix microstructure.

4.4. Laser processing

Laser processing has the advantages of high efficiency, high quality and wide processing range, so it has achieved rapid development in the field of industrial manufacturing. Because of the helical wavefront of OAM beams, the application of this kind of beams in the field of laser processing has attracted great attention of researchers. This section introduces the application of OAM beam in laser processing.

Chiral micro-nanostructures can obtain results more quickly and accurately in the chiral detection of yield-limited drugs, and can be used in optoelectronic materials and biological detection. Therefore, its manufacturing method is one of the current research hotspots. Chiral micro-nanostructures can be prepared by two-photon polymerization single-point method. However, the processing efficiency of this method is low, which results that it is difficult to achieve large-scale preparation of chiral structures. For this reason, the vortex beam based on spatial light modulator can be applied to the processing of chiral structures [213–215], and the number and direction of spiral blades can be controlled by changing the parameters of the computer-generated hologram. Li et al. superimposed the Laguerre Gaussian function to form spiral beams, and optimized the focus intensity of the double helix beams by the combination of double Gaussian function and step function [20]. Under intense focusing, a 10×10 double helix array with the period of $4 \mu\text{m}$ is prepared, as shown in Fig. 23. This method not only maintains the number of the helix structure, but also suppresses the sidelobe light intensity and reduces the bonding of the double helix structure. Liu et al. integrated the light beams into spiral light field, which reduced silver ions in one exposure and formed a metal double helix structure [21]. In order to

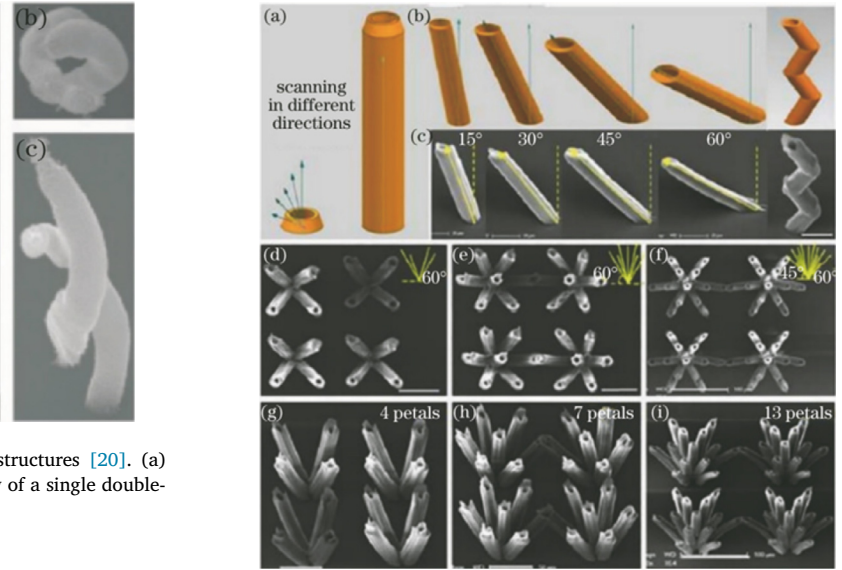


Fig. 25. 3D slant microtubes and flower-like microtube arrays fabricated by tilted the Bessel beam scanning [216].

reduce the influence of sidelobe, the experiment used a objective lens with high numerical aperture to separate the main lobe while keeping a high helix number. The results show that the silver double helix array shows obvious optical chirality, and the wavelength range is $3.5 \sim 8.5 \mu\text{m}$, as shown in Fig. 24.

In addition to the fabrication of chiral micro-nanostructures, the vortex beams with OAM can be used to emboss the morphology of polymers, which is expected to be used in the field of optical nanolithography. The induced spiral relief is very sensitive to the topological charge and wavefront of the OAM beam. On the basis of this theory, Ambrosio proposed that an azobenzene-containing polymer films can appear spiral relief pattern under focused Laguerre-Gaussian beam [214]. The results showed that the symmetry breaking on the polymer surface resulting in abnormal interference between the longitudinal and transverse components of the light field. The findings open up new possibilities for micron lithography and nanolithography based on azo polymers. Khonina analyzed the radiation characteristics of uniformly polarized beams with vortex phase and without that, and studied the effects on the microrelief formation of azo polymer films containing carbazole [215]. Especially, to eliminate the drawback that the shapes of the approximation and experimental microasperities differ significantly, author proposed to add the divergence gradient considered earlier as the third term, which has important reference value for future work.

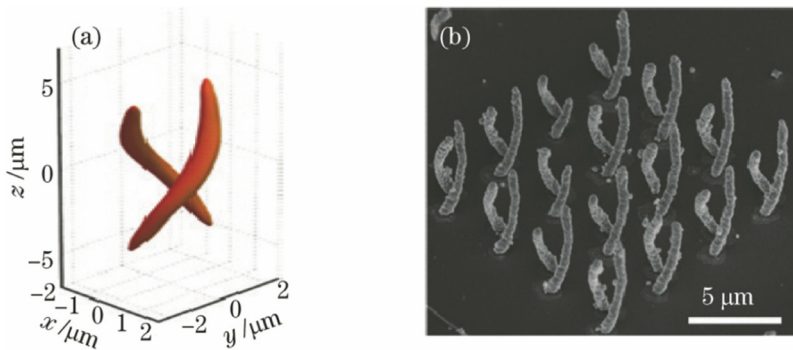


Fig. 24. Photoreduction of silver double helix with double-helix beam [21]. (a) Double-helix focal intensity distribution; (b) SEM images of an array of silver double helix; (c) measured transmittances of the double-helix silver array for left circular polarization and right circular polarization light at normal incidence.

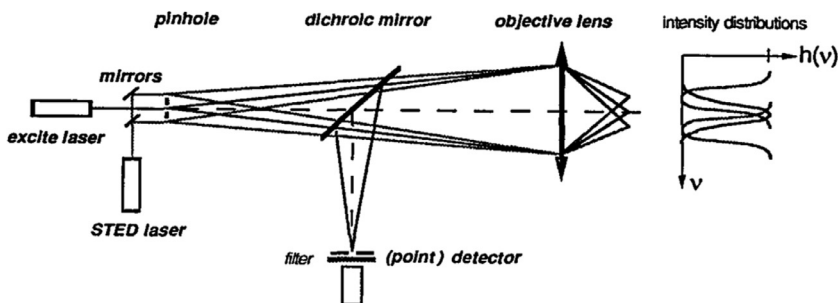


Fig. 26. Principles of a STED fluorescence scanning microscope [218].

In the field of laser processing, the Bessel beam based on spatial optical modulator has excellent processing advantages. The researchers use a spatial light modulator to shape the beams into high-order Bessel beams. Only by changing the cone lens radius r_0 and the topological charge n in the computer-generated hologram, the high-order Bessel beams with different diameters can be obtained. Combined with two-photon polymerization processing, high-order Bessel beam is successfully applied to pipeline processing to improve the processing efficiency and controllability of the pipeline structure. Yang et al. used spatial light modulator to shape femtosecond laser into high-order Bessel beam, and prepared oblique and bent pipes by setting different scanning directions [216]. As shown in Fig. 25, the pipes with angles of 15°, 30°, 45° and 60° and bent pipes were prepared, and the flower-shaped pipe array arrangement was realized. This processing method can accurately control the height of the micropipe by controlling the scanning speed and scanning time, but the surface roughness of the pipeline will increase due to the unevenness of exposure energy. In addition to Bessel beam, other non-diffracted beams such as Airy beam and Mathieu beam also have potential applications in the field of micro-nano processing. At present, the main research directions of Airy beam are optical properties and information transmission, and there are few studies on the micro-nano processing of Airy beam.

4.5. Super resolution imaging

When the topological charge of the OAM beam is low, there is a small spatial region (dark region) in the center of the vortex beam. Taking advantage of this feature, the OAM beam can also be used for super-resolution microscopic imaging [217]. In 1994, Hell and Wichmann proposed the method of "stimulated emission depletion (STED)" to improve the resolution of microscopic imaging, that is, the fluorescence is excited by a Gaussian beam, and another long-wavelength vortex beam overlapping with the Gaussian beam is used to suppress the fluorescence excitation through the electron level transfer. Therefore, the fluorescent spot is displayed only in the dark area of the vortex beam, which improves the imaging resolution. And this method breaks through the diffraction limit of light wave [218]. Fig. 26 depicts the setup of the proposed STED fluorescence scanning microscope. Based on this principle, a number of subsequent research groups have used vortex beams for super-resolution microscopic imaging [219–221].

Similarly, the imaged object can be scanned and imaged by Gaussian beam and vortex beam respectively, and then the two images can be subtracted to obtain an image with higher resolution and contrast [219,222] or extract the effective information of the imaged object [223–225]. For example, Swartzlander used the phase singularity of the spiral phase plate to filter the strong light, thus extracting the luminance information of the darker area of the object [223]; Fürhapter et al. used fork gratings to filter the image and restored the undulating morphology of the object surface [224].

In addition to microscopic imaging, in recent years, people have also begun to develop the application of OAM beam in radar imaging. Combining the OAM state with the algorithm, the resolution of radar imaging can be improved by optimizing the algorithm. On the one hand,

the OAM beams can be combined with the spectral estimation algorithm, which utilizes the approximate dual relationship between the OAM states and the azimuth of the target for radar imaging. On the other hand, OAM beams and sparse restoration algorithm are combined to realize radar imaging based on the orthogonal property of vortex beams in different OAM states. Liu et al. applied Sparse Bayesian Learning (SBL) algorithm to vortex radar imaging, and demonstrated the imaging results of Enhanced Sparse Bayesian Learning (ESBL) algorithm and Variational Bayesian Inference (VBI) algorithm in the presence of noise and grid mismatch. And they verified the range-azimuth two-dimensional imaging based on Sparse Bayesian Learning algorithm experimentally [226].

To sum up, OAM beam has great application prospects in the fields of ultra-high capacity optical communication, rotating body detection, optical tweezers, laser processing and super-resolution imaging, which will have a significant impact on technical science and basic science. Therefore, developing OAM beam generation technology and improving the technical level of OAM beam generation are very important for the application of OAM beam in the above fields and the development of wider application fields of OAM beam.

Summary

Based on previous studies and existing reports, the common categories of vortex beams carrying OAM, the current generation methods of OAM beams and their applications are reviewed in this paper. Generally speaking, there is still a lot of aspects for research in the generation scheme and application field of OAM beams. The new chiral atomic metamaterial synthesis process provides a wider choice of materials for the generation of OAM beams, which makes OAM beams expected to be used in aerospace fields. In addition, with the development of the processing and manufacturing industry, the scheme of generating OAM modes through photonic crystal fiber may not be limited to the theoretical simulation stage. The combination of OAM coding technology and Internet of things technology can further expand scope of application of OAM beams, such as in radio frequency identification devices technology [227]. At the same time, in the field of optical manipulation, if OAM beams are combined with artificial intelligence, it will be possible to make the particle manipulation technology in artificial intelligence faster and more accurate. In addition, the rapid development of crystal growth, chemical synthesis and optical fiber manufacturing technology may lead to the development of newer and customizable devices that generate OAM modes to adapt to the wider range of applications.

Funding

This work was supported by the National Natural Science Foundation of China (61905062, 61905061, 62075056 and 61927815), China Postdoctoral Science Foundation (2020M670613), Hebei Postdoctoral Scholarship Project (B2020003026), Hebei Science and Technology Innovation Strategy Project (2018E01). Thanks for the support of the Key Laboratory of all optical networks and advanced communications

networks of the Ministry of Education (Beijing Jiaotong University) (AON2019005).

Declaration of Competing Interest

No conflict of interest exists in the submission of this manuscript, and manuscript is approved by all authors for publication. I would like to declare on behalf of my co-authors that the article described was original manuscript that has not been published previously, and not under consideration for publication elsewhere, in whole or in part. All the authors listed have approved the manuscript that is enclosed.

Reference

- [1] Jackson JD. Classical electrodynamics. *Am J Phys* 1962;27(8):841–2.
- [2] Beth RA. Mechanical detection and measurement of the angular momentum of light. *Phys Rev* 1936;50(2):115–25.
- [3] John FN, Michael VB. Dislocations in wave trains. *Proc R Soc London Math Phys Sci* 1997;336(1605):165–90.
- [4] Allen L, Beijersbergen MW, Spreeuw RJ, Woerdman JP. Orbital angular momentum of light and the transformation of Laguerre-Gaussian laser modes. *Phys Rev A* 1992;45(11):8185–9.
- [5] Wang J, Yang JY, Fazal I, Ahmed N, Yan Y, Huang H, Ren Y, Yue Y, Dolinar S, Tur M, Willner A. Terabit free-space data transmission employing orbital angular momentum multiplexing. *Nat Photonics* 2012;6:488–96.
- [6] Gibson G, Courtial J, Padgett MJ, Vasnetsov M, Pas'ko V, Barnett SM, Franke AS. Free-space information transfer using light beams carrying orbital angular momentum. *Opt Express* 2004;12(22):5448–56.
- [7] Huang H, Xie G, Yan Y, Ahmed N, Ren Y, Yue Y, Rogawski D, Willner MJ, Erkmen BI, Birnbaum KM, Dolinar SJ, Lavery MPJ, Padgett MJ, Tur M, Willner AE. 100Tbit/s free-space data link enabled by three-dimensional multiplexing of orbital angular momentum, polarization, and wavelength. *Opt Lett* 2014;39(2):197–200.
- [8] Willner AE, Huang H, Yan Y, Ren Y, Ahmed N, Xie G, Bao C, Li L, Cao Y, Zhao Z, Wang J, Lavery MPJ, Tur M, Ramachandran S, Molisch AF, Ashrafi N, Ashrafi S. Optical communications using orbital angular momentum beams. *Adv Opt Photonics* 2015;7(1):66.
- [9] Wang A, Zhu L, Chen S, Du C, Mo Q, Wang J. Characterization of LDPC-coded orbital angular momentum modes transmission and multiplexing over a 50-km fiber. *Opt Express* 2016;24(11):11716–26.
- [10] Zhu L, Wang A, Chen S, Liu J, Mo Q, Du C, Wang J. Orbital angular momentum mode groups multiplexing transmission over 2.6-km conventional multi-mode fiber. *Opt Express* 2017;25(21):25637–45.
- [11] Li S, Wang J. Experimental demonstration of optical interconnects exploiting orbital angular momentum array. *Opt Express* 2017;25(18):21537–47.
- [12] Fu S, Zhai Y, Yin C, Zhou H, Gao C. Mixed orbital angular momentum amplitude shift keying through a single hologram. *OSA Continuum* 2018;1(2):295.
- [13] Fu S, Zhai Y, Zhou H, Zhang J, Wang T, Liu X, Gao C. Experimental demonstration of free-space multi-state orbital angular momentum shift keying. *Opt Express* 2019;27(23):33111–19.
- [14] Lavery MPJ, Speirs FC, Barnett SM, Padgett MJ. Detection of a spinning object using light's orbital angular momentum. *Science* 2013;341(6145):537.
- [15] Lavery MPJ, Barnett SM, Speirs FC, Padgett MJ. Observation of the rotational Doppler shift of a white-light, orbital-angular-momentum-carrying beam backscattered from a rotating body. *Optica* 2014;1(1):1–4.
- [16] Fu S, Wang T, Zhang Z, Zhai Y, Gao C. Non-diffractive Bessel-Gauss beams for the detection of rotating object free of obstructions. *Opt Express* 2017;25(17):20098–108.
- [17] Paterson L, Macdonald MP, Arlt J, Sibbett W, Bryant PE, Dholakia K. Controlled rotation of optically trapped microscopic particles. *Science* 2001;292(5518):912–14.
- [18] Dholakia K, Čižmár T. Shaping the future of manipulation. *Nat Photonics* 2011;5(6):335–42.
- [19] Padgett M, Bowman R. Tweezers with a twist. *Nat Photonics* 2011;5(6):343–8.
- [20] Yi Y, Liu L, Yang D, Zhang Q, Yang H, Gong Q. Femtosecond laser nano/microfabrication via three-dimensional focal field engineering. In: Proceeding of the SPIE; 2017, p. 10092.
- [21] Liu L, Yang D, Wan W, Yang H, Gong Q, Li Y. Fast fabrication of silver helical metamaterial with single-exposure femtosecond laser photoreduction. *Nanophotonics* 2019;8(6):1087–93.
- [22] Liu K, Cheng YQ, Gao Y, Li X, Qin YL, Wang HQ. Super-resolution radar imaging based on experimental OAM beams. *Appl Phys Lett* 2017;110(16):164102.
- [23] Zauderer E. Complex argument Hermite-Gaussian and Laguerre-Gaussian beams. *J Opt Soc Am A-Opt Image Sci Vis* 1986;3(4):465–9.
- [24] Kotlyar VV, Khonina SN, Almazov AA, Soifer VA, Jefimovs K, Turunen J. Elliptic Laguerre-Gaussian beams. *J Opt Soc Am A-Opt Image Sci Vis* 2006;23(1):43–56.
- [25] Zhang K, Wang Y, Yuan Y, Burokur SN. A review of orbital angular momentum vortex beams generation: from traditional methods to metasurfaces. *Appl Sci* 2020;10(3):1015.
- [26] Srinivas P, Raghu D, Anand V, Sruthy J, Amogh M, Awakash D, Nirmal KV, Balaji S, Shanti B. Generation and decomposition of scalar and vector modes carrying orbital angular momentum: a review. *Opt Eng* 2019;59(4):1–42.
- [27] Shen Y, Wang X, Xie Z, Min C, Fu X, Liu Q, Gong M, Yuan X. Optical vortices 30 years on: OAM manipulation from topological charge to multiple singularities. *Light: Sci Appl* 2019;8(1):90.
- [28] Enderlein J, Pampaloni F. Unified operator approach for deriving Hermite-Gaussian and Laguerre-Gaussian laser modes. *J Opt Soc Am A-Opt Image Sci Vis* 2004;21(8):1553–8.
- [29] Kim H, Lee YH. Hermite-Gaussian and Laguerre-Gaussian beams beyond the paraxial approximation. *Opt Commun* 1999;169(1):9–16.
- [30] Zhou G. Analytical vectorial structure of Laguerre-Gaussian beam in the far field. *Opt Lett* 2006;31(17):2616–18.
- [31] Qu J, Zhong Y, Cui Z, Cai Y. Elegant Laguerre-Gaussian beam in a turbulent atmosphere. *Opt Commun* 2010;283(14):2772–81.
- [32] Cao J, Chen Q, Guo H. Creation of a controllable three dimensional optical chain by TEM₀₁ mode radially polarized Laguerre-Gaussian beam. *Optik (Stuttg)* 2013;124(15):2033–6.
- [33] Ishaaya AA, Eckhouse V, Shimshi L, Davidson N, Friesem AA. Intracavity coherent addition of single high-order modes. *Opt Lett* 2005;30(14):1770–2.
- [34] Protasov CE, Gusearov AV. Modeling the effect of beam shaping at selective laser melting. *Procedia IUTAM* 2017;23:147–54.
- [35] Durin J. Exact solutions for non-diffracting beams. I. The scalar theory. *J Opt Soc Am A* 1987;4(4):651–4.
- [36] McGloin D, Dholakia K. Bessel beams: diffraction in a new light. *Contemp Phys* 2005;46(1):15–28.
- [37] Turunen J, Vasara A, Friberg AT. Holographic generation of diffraction-free beams. *Appl Opt* 1988;27(19):3959–62.
- [38] Garcés CV, McGloin D, Melville H, Sibbett W, Dholakia K. Simultaneous micromanipulation in multiple planes using a self-reconstructing light beam. *Nature* 2002;419(6903):145–7.
- [39] Volkesepulveda K, Garcéschavez V, Chávezcerda S, Arlt J, Dholakia K. Orbital angular momentum of a high-order Bessel light beam. *J Opt B-Quant Semiclass Opt* 2002;4(2):223–4.
- [40] Brzobohatý O, Čižmar T, Zemanek P. High quality quasi-Bessel beam generated by round-trip axicon. *Opt Express* 2008;16(17):12688–700.
- [41] Arlt J, Garcéschavez V, Sibbett W, Dholakia K. Optical micromanipulation using a Bessel light beam. *Opt Commun* 2001;197(4):239–45.
- [42] Bouchal Z, Wagner J, Chlup M. Self-reconstruction of a distorted nondiffracting beam. *Opt Commun* 1998;151(4):207–11.
- [43] Saad F, El HEM, Belafhal A. Generation of generalized spiraling Bessel beams of arbitrary order by curved fork-shaped holograms. *Opt Quantum Electr* 2016;48(10):454.
- [44] Gori F, Guattari G, Padovani C. Bessel-Gauss beams. *Opt Commun* 1987;64(6):491–5.
- [45] Durin J, Miceli JJ, Eberly JH. Comparison of Bessel and Gaussian beams. *Opt Lett* 1988;13(2):79–80.
- [46] Zahid M, Zubairy MS. Directionality of partially coherent Bessel-Gauss beams. *Opt Commun* 1989;70(5):361–4.
- [47] Liu S, Song Z, Huang X, Shi D, Jiang M, Sui Q, Feng D. Transmission analysis of off-axis high order Bessel-Gaussian vortex beam. *J Atmos Environ Opt* 2019;14(6):401–10.
- [48] Lu XH, Chen XM, Zhang L, Xue DJ. High-order Bessel-Gaussian beam and its propagation properties. *Chin Phys Lett* 2003;20(12):2155–7.
- [49] Khonina SN, Kotlyar VV, Skidanov RV, Soifer VA, Jefimovs K, Simonen J, Turunen J. Rotation of microparticles with Bessel beams generated by diffractive elements. *J Mod Opt* 2004;51(14):2167–84.
- [50] Greene PL, Hall DG. Properties and diffraction of vector Bessel-Gauss beams. *J Opt Soc Am A* 1998;15(12):3020–7.
- [51] Arlt J, Dholakia K. Generation of high-order Bessel beams by use of an axicon. *Opt Commun* 2000;177(1):297–301.
- [52] Chen B, Chen Z, Pu J. Propagation of partially coherent Bessel-Gaussian beams in turbulent atmosphere. *Opt Laser Technol* 2008;40(6):820–7.
- [53] Wang X, Lü B. The beam propagation factor and far-field distribution of Bessel-modulated Gaussian beams. *Opt Quantum Electr* 2002;34(11):1071–7.
- [54] Çil CZ, Eyyuboğlu HT, Baykal Y, Korotkova O, Cai Y. Beam wander of J₀- and J₁-Bessel Gaussian beams propagating in turbulent atmosphere. *Appl Phys B* 2010;98(1):195–202.
- [55] Gori F, Santarsiero M, Borghi R, Guattari G. Intensity-based modal analysis of partially coherent beams with Hermite-Gaussian modes. *Opt Lett* 1998;23(13):989–91.
- [56] Yu J, Chen Y, Liu L, Liu X, Cai Y. Splitting and combining properties of an elegant Hermite-Gaussian correlated Schell-model beam in Kolmogorov and non-Kolmogorov turbulence. *Opt Express* 2015;23(10):13467–81.
- [57] Viswanathan NK, Inavalli VVG. Generation of optical vector beams using a two-mode fiber. *Opt Lett* 2009;34(8):1189–91.
- [58] Kotlyar VV, Kovalev AA, Porfirev AP. Vortex Hermite-Gaussian laser beams. *Opt Lett* 2015;40(5):701–4.
- [59] Li P, Zhang Y, Liu S, Ma C, Han L, Cheng H, Zhao J. Generation of perfect vectorial vortex beams. *Opt Lett* 2016;41(10):2205–8.
- [60] Chen M, Mazilu M, Arita Y, Wright EM, Dholakia K. Dynamics of microparticles trapped in a perfect vortex beam. *Opt Lett* 2013;38(22):4919–22.
- [61] Vaity P, Rusch L. Perfect vortex beam: fourier transformation of a Bessel beam. *Opt Lett* 2015;40(4):597–600.
- [62] Ostrovsky AS, Rickenstorff PC, Arrizón V. Generation of the “perfect” optical vortex using a liquid-crystal spatial light modulator. *Opt Lett* 2013;38(4):534–536.
- [63] Khonina SN, Balalayev SA, Skidanov RV, Kotlyar VV, Päiväranta B, Turunen J. Encoded binary diffractive element to form hyper-geometric laser beams. *J Opt A: Pure Appl Opt* 2009;11(6):065702.
- [64] Ganchevskaya SV, Skidanov RV. Vortex axicons for hypergeometric beams formation. *Procedia Eng* 2017;201:135–40.

- [65] Kotlyar VV, Kovalev AA, Skidanov RV, Khonina SN, Turunen J. Generating hypergeometric laser beams with a diffractive optical element. *Appl Opt* 2008;47(32):6124–33.
- [66] Skidanov RV, Khonina SN, Morozov AA. Optical rotation of microparticles in hypergeometric beams formed by diffraction optical elements with multilevel microrelief. *J Opt Technol* 2013;80(10):585–9.
- [67] Panagiotopoulos P, Couairon A, Kolesik M, Papazoglou DG, Moloney JV, Tzortzakis S. Nonlinear plasma-assisted collapse of ring-Airy wave packets. *Phys Rev A* 2016;93(3):033808.
- [68] Manousidakis M, Papazoglou DG, Farsari M, Tzortzakis S. Abruptly autofocusing beams enable advanced multiscale photo-polymerization. *Optica* 2016;3(5):525–30.
- [69] Lu W, Sun X, Chen H, Liu S, Lin Z. Abruptly autofocusing property and optical manipulation of circular Airy beams. *Phys Rev A* 2019;99(1):013817.
- [70] Jiang Y, Huang K, Lu X. Radiation force of abruptly autofocusing Airy beams on a Rayleigh particle. *Opt Express* 2013;21(20):24413–21.
- [71] Khonina SN, Porfirev AP, Ustinov AV, Butt MA. Generation of complex transverse energy flow distributions with autofocusing optical vortex beams. *Micromachines (Basel)* 2021;12(3):297.
- [72] Jiang Y, Huang K, Lu X. Propagation dynamics of abruptly autofocusing Airy beams with optical vortices. *Opt Express* 2012;20(17):18579–84.
- [73] Dai HT, Liu YJ, Luo D, Sun XW. Propagation dynamics of an optical vortex imposed on an Airy beam. *Opt Lett* 2010;35(23):4075–7.
- [74] Dai HT, Liu YJ, Luo D, Sun XW. Propagation properties of an optical vortex carried by an Airy beam: experimental implementation. *Opt Lett* 2011;36(9):1617–1619.
- [75] Chen RP, Zhong LX, Wu Q, Chew KH. Propagation properties and M2 factors of a vortex Airy beam. *Opt Laser Technol* 2012;44(7):2015–19.
- [76] Chen RP, Chew KH, He S. Dynamic control of collapse in a vortex airy beam. *Sci Rep* 2013;3(1):1406.
- [77] Davis JA, Cottrell DM, Sand D. Abruptly autofocusing vortex beams. *Opt Express* 2012;20(12):13302–10.
- [78] Chen RP, Ooi CHR. Nonclassicality of vortex Airy beams in the Wigner representation. *Phys Rev A* 2011;84(4):043846.
- [79] Wang D, Jin L, Rosales GC, Gao W. Generating arbitrary arrays of circular Airy Gaussian vortex beams with a single digital hologram. *Appl Phys B* 2021;127(2):22.
- [80] Chen X, Deng D, Zhuang J, Peng X, Li D, Zhang L, Zhao F, Yang X, Liu H, Wang G. Focusing properties of circle Pearcey beams. *Opt Lett* 2018;43(15):3626–9.
- [81] Wang C, Ren Y, Liu T, Liu Z, Qiu S, Li Z, Ding Y, Wu H. Generating a new type of polygonal perfect optical vortex. *Opt Express* 2021;29(9):14126–34.
- [82] Ren Y, Wang C, Liu T, Wang Z, Yin C, Qiu S, Li Z, Wu H. Polygonal shaping and multi-singularity manipulation of optical vortices via high-order cross-phase. *Opt Express* 2020;28(18):26257–66.
- [83] Ring JD, Lindberg J, Mourka A, Mazilu M, Dholakia K, Dennis MR. Auto-focusing and self-healing of Pearcey beams. *Opt Express* 2012;20(17):18955–66.
- [84] Peng Y, Chen C, Chen B, Peng X, Zhou M, Zhang L, Li D, Deng D. Propagation of a Pearcey–Gaussian-vortex beam in free space and Kerr media. *Laser Phys* 2016;26(12):125401.
- [85] Ma H, Li X, Tai Y, Li H, Wang J, Tang M, Tang J, Wang Y, Nie Z. Generation of circular optical vortex array. *Ann Phys* 2017;529(12):1700285.
- [86] Yu J, Zhou C, Jia W, Hu A, Cao W, Wu J, Wang S. Three-dimensional Dammann vortex array with tunable topological charge. *Appl Opt* 2012;51(13):2485–90.
- [87] Migara LK, Lee CM, Kwak K, Lee H, Song JK. Tunable optical vortex arrays using spontaneous periodic pattern formation in nematic liquid crystal cells. *Curr Appl Phys* 2018;18(7):819–23.
- [88] Wei GX, Lu LL, Guo CS. Generation of optical vortex array based on the fractional Talbot effect. *Opt Commun* 2009;282(14):2665–9.
- [89] Srinivas P, Shankar P, Srinivasan B. Investigation of fractional charge OAM beam generation and its decomposition. In: Progress in electromagnetic research symposium (PIERS); 2016. p. 806–10.
- [90] Ni R, Niu YF, Du L, Hu XP, Zhang Y, Zhu SN. Topological charge transfer in frequency doubling of fractional orbital angular momentum state. *Appl Phys Lett* 2016;109(15):151103.
- [91] Zhu G, Liu Z, Fu C, Liu S, Bai Z, Wang Y. High-Precise fractional orbital angular momentum probing with a fiber grating tip. *J Lightwave Technol* 2021;39(6):1867–72.
- [92] Dai K, Miller JK, Li W, Watkins RJ, Johnson EG. Fractional orbital angular momentum conversion in second-harmonic generation with an asymmetric perfect vortex beam. *Opt Lett* 2021;46(14):3332–5.
- [93] Wang X, Nie Z, Liang Y, Wang J, Li T, Jia B. Recent advances on optical vortex generation. *Nanophotonics* 2018;7(9):1533–56.
- [94] Shen Y, Wan Z, Meng Y, Fu X, Gong M. Polygonal Vortex Beams. *IEEE Photonics J* 2018;10(4):1–16.
- [95] Smith PW. Mode selection in lasers. *Proc IEEE* 1972;60(4):422–40.
- [96] Tamm C, Weiss CO. Bistability and optical switching of spatial patterns in a laser. *J Opt Soc Am B* 1990;7(6):1034–8.
- [97] Tamm C. Frequency locking of two transverse optical modes of a laser. *J Phys A Gen Phys* 1988;38(11):S960–3.
- [98] Hemsing E, Marinelli A, Rosenzweig JB. Generating optical orbital angular momentum in a high-gain free-electron laser at the first harmonic. *Phys Rev Lett* 2011;106(16):164803.
- [99] Kim DJ, Kim JW. Direct generation of an optical vortex beam in a single-frequency Nd:YVO₄ laser. *Opt Lett* 2015;40(3):399–402.
- [100] Zhang L, Geng T, Gao X, Zhuang S, Lian J. Formation of high-quality vortex laser beams with different orbital angular momenta in the laser resonator. *J Opt Soc Am A* 2018;35(9):1599–603.
- [101] Liu SS, Chen XD, Pu JX, Lin ZL, Chen ZY. A v-folded digital laser for on-demand vortex beams by astigmatic transformation of Hermite–Gaussian modes. *Chin Phys Lett* 2019;36(12):124203.
- [102] Ngcobo S, Litvin I, Burger L, Forbes A. A digital laser for on-demand laser modes. *Nat Commun* 2013;4(4):2289.
- [103] Veinhard M, Bellanger S, Daniault L, Fsaifes I, Bourderionnet J, Larat C, Lallier E, Brignon A, Chanteloup JC. Orbital angular momentum beams generation from 61 channels coherent beam combining femtosecond digital laser. *Opt Lett* 2021;46(1):25–8.
- [104] Zhou N, Liu J, Wang J. Reconfigurable and tunable twisted light laser. *Sci Rep* 2018;8(1):11394.
- [105] Forbes A. Structured Light from Lasers. *Laser Photon Rev* 2019;13(11):1900140.
- [106] Gao MW, Gao CQ, Lin ZF. Generation of twisted stigmatic beam and transfer of orbital angular momentum during the beam transformation. *Acta Phys Sin Chin Ed* 2007;56(4):2184–90.
- [107] Zhang HX, Zhao H. Orbital angular momentum of high-order elliptical Hermite–Gaussian beams. *Acta Photon Sin* 2008;37(8):1679–83.
- [108] Lee J, Arita Y, Toyoshima S, Miyamoto K, Panagiotopoulos P, Wright EM, Dholakia K, Omatsu T. Photopolymerization with light fields possessing orbital angular momentum: generation of helical microfibers. *ACS Photonics* 2018;5(10):4156–4163.
- [109] Abramochkin E, Volostnikov V. Beam transformations and nontransformed beams. *Opt Commun* 1991;83(1):123–35.
- [110] Beijersbergen MW. Astigmatic laser mode converters and transfer of orbital angular momentum. *Opt Commun* 1993;96(1):123–32.
- [111] Lu J, Meng L, Shi F, Liu X, Luo Z, Yan P, Huang L, Pang F, Wang T, Zeng X, Zhou P. Dynamic mode-switchable optical vortex beams using acousto-optic mode converter. *Opt Lett* 2018;43(23):5841–4.
- [112] Gao CQ. Generation of the stigmatic beam with orbital angular momentum. *Chin Phys Lett* 2001;18(6):771–3.
- [113] Zhao J, Chremmos ID, Song D, Christodoulides DN, Efremidis NK, Chen Z. Curved singular beams for three-dimensional particle manipulation. *Sci Rep* 2015;5(1):12086.
- [114] Grier DG. A revolution in optical manipulation. *Nature* 2003;424(6950):810–16.
- [115] Tamburini F, Thidé B, Molina-Terriza G, Anzolin G. Twisting of light around rotating black holes. *Nat Phys* 2011;7(3):195–7.
- [116] Hui X, Zheng S, Hu Y, Xu C, Jin X, Chi H, Zhang X. Ultralow reflectivity spiral phase plate for generation of millimeter-wave OAM beam. *IEEE Antennas Wirel Propag Lett* 2015;14(14):966–9.
- [117] Khonina SN, Kotlyar VV, Shinkaryev MV, Soifer VA, Uspleniev GV. The phase rotor filter. *J Mod Opt* 1992;39(5):1147–54.
- [118] Schemmel P, Pisano G, Maffei B. Modular spiral phase plate design for orbital angular momentum generation at millimetre wavelengths. *Opt Express* 2014;22(12):14712–26.
- [119] Kotlyar VV, Almazov AA, Khonina SN, Soifer VA, Elfstrom H, Turunen J. Generation of phase singularity through diffracting a plane or Gaussian beam by a spiral phase plate. *J Opt Soc Am A* 2005;22(5):849–61.
- [120] Kovalev AA, Kotlyar VV. Orbital angular momentum of an elliptic beam after an elliptic spiral phase plate. *J Opt Soc Am A* 2019;36(1):142–8.
- [121] Cheng L, Hong W, Hao ZC. Generation of electromagnetic waves with arbitrary orbital angular momentum modes. *Sci Rep* 2014;4(1):4814.
- [122] Zhou Y, Gao H, Teng J, Luo X, Hong M. Orbital angular momentum generation via a spiral phase microsphere. *Opt Lett* 2018;43(1):34–7.
- [123] Massari M, Ruffato G, Gintoli M, Ricci F, Romanato F. Fabrication and characterization of high-quality spiral phase plates for optical applications. *Appl Opt* 2015;54(13):4077–83.
- [124] Debernardi P, Tibaldi A, Gerlach P, Martelli P, Boffi P, Martinelli M, Coville D, Orta R. Modal performance of spiral phase plate VCSELs. *IEEE J Quantum Electron* 2016;52(5):1–8.
- [125] Bazhenov VY, Soskin MS, Vasnetsov MV. Screw Dislocations in Light Wavefronts. *J Mod Opt* 1992;39(5):985–90.
- [126] Li S, Wang J. Simultaneous demultiplexing and steering of multiple orbital angular momentum modes. *Sci Rep* 2015;5(1):15406.
- [127] Kong F, Zhang C, Bouchard F, Li Z, Brown GG, Ko DH, Hammond TJ, Arissian L, Boyd RW, Karimi E, Corkum PB. Controlling the orbital angular momentum of high harmonic vortices. *Nat Commun* 2017;8(1):14970.
- [128] JK Yamming LiAnd Michael J. Escutti. Orbital angular momentum generation and mode transformation with high efficiency using forked polarization gratings. *Appl Opt* 2012;51(34):8236–45.
- [129] Xiao Q, Klitis C, Li S, Chen Y, Cai X, Sorel M, Yu S. Generation of photonic orbital angular momentum superposition states using vortex beam emitters with superimposed gratings. *Opt Express* 2016;24(4):3168–76.
- [130] Zheng S, Hui X, Zhu J, Chi H, Jin X, Yu S, Zhang X. Orbital angular momentum mode-demultiplexing scheme with partial angular receiving aperture. *Opt Express* 2015;23(9):12251–7.
- [131] Ge SJ, Ji W, Cui GX, Wei BY, Hu W, Lu YQ. Fast switchable optical vortex generator based on blue phase liquid crystal fork grating. *Opt Mater Express* 2014;4(12):2535–41.
- [132] Lee JCT, Alexander SK, Kevan SD, Roy S, Memoran BJ. Laguerre–Gauss and Hermite–Gauss soft X-ray states generated using diffractive optics. *Nat Photonics* 2019;13(3):205–9.
- [133] Stoyanov L, Topuzoski S, Stefanov I, Janicijevic L, Dreischuh A. Far field diffraction of an optical vortex beam by a fork-shaped grating. *Opt Commun* 2015;350(1):301–8.

- [134] Su M, Liu J, He Y, Chen S, Li Y. Optical orbital angular momentum demultiplexing and channel equalization by using equalizing Dammann vortex grating. *Adv Condens Matter Phys* 2017;2017:6293910.
- [135] Yu J, Zhou C, Jia W, Wu J, Zhu L, Lu Y, Xiang C, Li S. Generation of controllable rotating petal-like modes using composited Dammann vortex gratings. *Appl Opt* 2015;54(7):1667.
- [136] Lei T, Zhang M, Li Y, Jia P, Liu GN, Xu X, Li Z, Min C, Lin J, Yu C, Niu H, Yuan X. Massive individual orbital angular momentum channels for multiplexing enabled by Dammann gratings. *Light: Sci Appl* 2015;4(3):e257.
- [137] Qiu J, Shen B, Zhang X, Bu Z, Yi L, Zhang L, Xu Z. Vortex beam of tilted orbital angular momentum generated from grating. *Plasma Phys Control Fusion* 2019;61(10):105001.
- [138] Detani T, Zhao H, Wang P, Suzuki T, Li H. Simultaneous generation of the second- and third-order OAM modes by using a high-order helical long-period fiber grating. *Opt Lett* 2021;46(5):949–52.
- [139] Zheng S, Wang J. Measuring orbital angular momentum (OAM) states of vortex beams with annular gratings. *Sci Rep* 2017;7(1):40781.
- [140] Guo CS, Liu X, Ren XY, Wang HT. Optimal annular computer-generated holograms for the generation of optical vortices. *J Opt Soc Am A* 2005;22(2):385–90.
- [141] Guo CS, Liu X, He JL, Wang HT. Optimal annulus structures of optical vortices. *Opt Express* 2004;12(19):4625–34.
- [142] Gu B, Hu Y, Zhang X, Li M, Zhu Z, Rui G, He J, Cui Y. Angular momentum separation in focused fractional vector beams for optical manipulation. *Opt Express* 2021;29(10):14705–19.
- [143] Yao E, Franke AS, Courtial J, Padgett MJ, Barnett SM. Observation of quantum entanglement using spatial light modulators. *Opt Express* 2006;14(26):13089–94.
- [144] Ren Y, Li L, Wang Z, Kamali SM, Arbab E, Arbab A, Zhao Z, Xie G, Cao Y, Ahmed N, Yan Y, Liu C, Willner AJ, Ashrafi S, Tur M, Faraon A, Willner AE. Orbital angular momentum-based space division multiplexing for high-capacity underwater optical communications. *Sci Rep* 2016;6(1):33306.
- [145] Qin F, Wan L, Li L, Zhang H, Wei G, Gao S. A transmission metasurface for generating OAM beams. *IEEE Antennas Wirel Propag Lett* 2018;17(10):1793–6.
- [146] Bai X, Kong F, Sun Y, Wang G, Qian J, Li X, Cao A, He C, Liang XL, Jin R, Zhu W. High-efficiency transmissive programmable metasurface for multimode OAM generation. *Adv Opt Mater* 2020;8(17):4281–91.
- [147] Zhou N, Wang J. Metasurface-assisted orbital angular momentum carrying Bessel-Gaussian Laser: proposal and simulation. *Sci Rep* 2018;8(1):8038.
- [148] Li G, Kang M, Chen S, Zhang S, Pun EYB, Cheah KW, Li J. Spin-enabled plasmonic metasurfaces for manipulating orbital angular momentum of light. *Nano Lett.* 2013;13(9):4148–51.
- [149] Karimi E, Schulz S, De Leon I, Qassim H, Upham J, Boyd R. Generating optical orbital angular momentum at visible wavelengths using a plasmonic metasurface. *Light: Sci Appl* 2014;3:e167.
- [150] Yang Y, Wang W, Moitra P, Kravchenko II, Briggs DP, Valentine J. Dielectric meta-reflectarray for broadband linear polarization conversion and optical vortex generation. *Nano Lett.* 2014;14(3):1394–9.
- [151] Jiang S, Chen C, Zhang H, Chen W. Achromatic electromagnetic metasurface for generating a vortex wave with orbital angular momentum (OAM). *Opt Express* 2018;26(5):6466–77.
- [152] Xu Y, Sun J, Frantz J, Shalaev MI, Walasik W, Pandey A, Myers JD, Bekele RY, Tsukernik A, Sanghera JS, Litchinitser NM. Reconfiguring structured light beams using nonlinear metasurfaces. *Opt Express* 2018;26(23):30930–43.
- [153] Du J, Wang J. Dielectric metasurfaces enabling twisted light generation/detection/(de)multiplexing for data information transfer. *Opt Express* 2018;26(10):13183–94.
- [154] Qi X, Zhang Z, Tong X, Que X, Nie Z, Hu J. Generating dual-mode dual-polarization OAM based on transmissive metasurface. *IEEE Int Conf Comput Electromagn* 2019;9(1):1–3.
- [155] Yang Y, Thirunavukkarasu G, Babiker M, Yuan J. Orbital-angular-momentum mode selection by rotationally symmetric superposition of chiral states with application to electron vortex beams. *Phys Rev Lett* 2017;119(9):094802.
- [156] Hu T, Wang Y, Ma B, Zhang J. Orbit angular momentum MIMO with mode selection for UAV-assisted A2G networks 2020; 20(8):2289.
- [157] Clark CW, Barankov R, Huber MG, Arif M, Cory DG, Pushin DA. Controlling neutron orbital angular momentum. *Nature* 2015;525(7570):504–6.
- [158] Li J, Liu J, Hu H, Zhao Y, Xia F. Tunable orbital angular momentum mode conversion in asymmetric long period fiber gratings. *IEEE Photon Technol Lett* 2017;29(23):2103–6.
- [159] Saitoh K, Hasegawa Y, Hirakawa K, Tanaka N, Uchida M. Measuring the orbital angular momentum of electron vortex beams using a forked grating. *Phys Rev Lett* 2013;111(7):074801.
- [160] Deepa S, Ram BSB, Senthilkumaran P. Helicity dependent diffraction by angular momentum transfer. *Sci Rep* 2019;9(1):12491.
- [161] Chu C, Gao S, Liu Z, Tu J, Yang J, Hao C, Liu W, Li Z. Hybrid angular gradient phase grating for measuring the orbital angular momentum of perfect optical vortex beams. *IEEE Photonics J* 2020;12(3):7902409.
- [162] Khilo NA. Diffraction and order conversion of Bessel beams in uniaxial crystals. *Opt Commun* 2012;285(5):503–9.
- [163] Khilo NA, Petrova ES, Ryzhevich AA. Transformation of the order of Bessel beams in uniaxial crystals. *Quantum Elec (Woodbury)* 2001;31(1):85–9.
- [164] Khonina S, Morozov A, Karpeev S. Effective transformation of a zero-order Bessel beam into a second-order vortex beam using a uniaxial crystal. *Laser Phys* 2014;24(5):056101.
- [165] Marrucci L, Manzo C, Paparo D. Optical spin-to-orbital angular momentum conversion in inhomogeneous anisotropic media. *Phys Rev Lett* 2006;96(16):163905.
- [166] Yang H, Chen ZQ, Liu Q, Hu YQ, Duan HG. Near-field orbital angular momentum generation and detection based on spin-orbit interaction in gold metasurfaces. *Adv Theory SImul* 2019;2(10):1900133.
- [167] Spektor G, Kilbane D, Mahro AK, Hartelt M, Prinz E, Aeschlimann M, Orenstein M. Mixing the light spin with plasmon orbit by nonlinear light-matter interaction in gold. *Phys Rev X* 2019;9(2):021031.
- [168] Zhou H, Dong J, Zhou Y, Zhang J, Liu M, Zhang X. Designing appointed and multiple focuses with plasmonic vortex lenses. *IEEE Photonics J* 2015;7(4):1–7.
- [169] Qi Z, Peiyu L, Yanying L, Han W, Lixia L, Liren Z, Shuyun T. Optical vortex generator with linearly polarized light illumination. *J Nanophotonics* 2018;12(1):1–7.
- [170] Tsai WY, Huang JS, Huang CB. Selective trapping or rotation of isotropic dielectric micro-particles by optical near field in a plasmonic archimedes spiral. *Nano Lett.* 2014;14(2):547–52.
- [171] Yang J, Zhang H, Zhang X, Chen Z, Xi L, Zhang W. A hollow-core circular photonic crystal fiber mode selective coupler for generating orbital angular momentum modes. *Opt Fiber Technol* 2021;64:102543.
- [172] Yang J, Liu H, Pang F, Wen J, Zheng H, Chen L, He X, Shang Y, Chen N, Li Y, Wang T. All-fiber multiplexing and transmission of high-order circularly polarized orbital angular momentum modes with mode selective couplers. *IEEE Photonics J* 2019;11(3):1–9.
- [173] Yao S, Ren G, Shen Y, Jiang Y, Zhu B, Jian S. Tunable orbital angular momentum generation using all-fiber fused coupler. *IEEE Photon Technol Lett* 2018;30(11):99–102.
- [174] Li L, Zhu S, Li J, Shao X, Galvanauskas A, Ma X. All-in-fiber method of generating orbital angular momentum with helically symmetric fibers. *Appl Opt* 2018;57(28):8182–6.
- [175] Jiang Y, Ren G, Shen Y, Xu Y, Jin W, Wu Y, Jian W, Jian S. Two-dimensional tunable orbital angular momentum generation using a vortex fiber. *Opt Lett* 2017;42(23):5014–17.
- [176] Pidishety S, Pachava S, Gregg P, Ramachandran S, Brambilla G, Srinivasan B. Orbital angular momentum beam excitation using an all-fiber weakly fused mode selective coupler. *Opt Lett* 2017;42(21):4347–50.
- [177] Zhang H, Zhang X, Li H, Deng Y, Xi L, Tang X, Zhang W. The orbital angular momentum modes supporting fibers based on the photonic crystal fiber structure. *Crystals* 2017;7(10):286.
- [178] Seghilani M, Azanza J. All-fiber OAM generation/conversion using helically patterned photonic crystal fiber. *IEEE Photon Technol Lett* 2018;30(4):347–50.
- [179] Israk MF, Razzak MA, Ahmed K, Hassan MM, Kabir MA, Hossain MN, Paul BK, Dhasarathan V. Ring-based coil structure photonic crystal fiber for transmission of orbital angular momentum with large bandwidth: outline, investigation and analysis. *Opt Commun* 2020;473(15):126003.
- [180] Hassan M, Kabir MA, Hossain M, Biswas B, Paul BK. Photonic crystal fiber for robust orbital angular momentum transmission: design and investigation. *Opt Quantum Electr* 2019;52(1):8.
- [181] Kabir MA, Ahmed K, Hassan MM, Hossain MM, Paul BK. Design a photonic crystal fiber of guiding terahertz orbital angular momentum beams in optical communication. *Opt Commun* 2020;475(15):126192.
- [182] Hassan M, Kabir MA, Hossain M, Nguyen TK, Paul BK, Dhasarathan V. Numerical analysis of circular core shaped photonic crystal fiber for orbital angular momentum with efficient transmission. *Appl Phys B* 2020;126(9):145.
- [183] Liu E, Tan W, Yan B, Xie J, Ge R, Liu J. Robust transmission of orbital angular momentum mode based on a dual-cladding photonic quasi-crystal fiber. *J Phys D Appl Phys* 2019;52(32):325110.
- [184] Brasselet E, Izdebskaya Y, Shvedov V, Desyatnikov AS, Krolikowski W, Kivshar YS. Dynamics of optical spin-orbit coupling in uniaxial crystals. *Opt Lett* 2009;34(7):1021–3.
- [185] Fadelyeva TA, Volyar AV. Extreme spin-orbit coupling in crystal-traveling paraxial beams. *J Opt Soc Am A* 2010;27(3):381–9.
- [186] Li H, Ren G, Lian Y, Zhu B, Tang M, Zhao Y, Jian S. Broadband orbital angular momentum transmission using a hollow-core photonic bandgap fiber. *Opt Lett* 2016;41(15):3591–4.
- [187] Jiang Y, Ren G, Lian Y, Zhu B, Jin W, Jian S. Tunable orbital angular momentum generation in optical fibers. *Opt Lett* 2016;41(15):3535–8.
- [188] Fazaea Y, Mezhuyev V. Selective mode excitation techniques for mode-division multiplexing: a critical review. *Opt Fiber Technol* 2018;45:280–8.
- [189] Huang YT, Su DC, Tsai YK. Wavelength division multiplexing and demultiplexing by using a substrate-mode grating pair. *Opt Lett* 1992;17(22):1629–31.
- [190] Wang J, Yang JY, Fazal IM, Ahmed N, Yan Y, Huang H, Ren Y, Yue Y, Dolinar S, Tur M, Willner AE. Terabit free-space data transmission employing orbital angular momentum multiplexing. *Nat Photonics* 2012;6(7):488–96.
- [191] Jeong JH, Jeong JM. Binary amplitude shift keying based signal processing for brilouin optical correlation domain analysis. *J Korean Phys Soc* 2012;61(12):1975–1980.
- [192] Indriyanto S, Fitrian IA, Hendry J, Yosef I. Underwater data transmission using frequency shift keying (FSK) modulation with bit rate of 2400bps. *Bull Pos dan Telekomunikasi* 2020;18(1):17–28.
- [193] Heinisch C, Lichtenberg S, Petrov V, Petter J, Tschudi T. Phase-shift keying of an optical Bragg cell filter. *Opt Commun* 2005;253(4):320–31.
- [194] Li G, Zentgraf T, Zhang S. Rotational Doppler effect in nonlinear optics. *Nat Phys* 2016;12(8):736–40.
- [195] Smolin AL. Doppler effect in a rotating frame. *Soviet Physics Journal* 1990;33(7):565–8.
- [196] Nienhuis G. Doppler effect induced by rotating lenses. *Opt Commun* 1996;132(1):8–14.
- [197] Qiu S, Liu T, Li Z, Wang C, Ren Y, Shao Q, Xing C. Influence of lateral misalignment on the optical rotational Doppler effect. *Appl Opt* 2019;58(10):2650–5.

- [198] Zhou HL, Fu DZ, Dong JJ, Zhang P, Chen DX, Cai XL, Li FL, Zhang XL. Orbital angular momentum complex spectrum analyzer for vortex light based on the rotational Doppler effect. *Light: Sci Appl* 2017;6(4):16251.
- [199] Anderson AQ, Strong EF, Heffernan BM, Siemens ME, Rieker GB, Gopinath JT. Observation of the rotational Doppler shift with spatially incoherent light. *Opt Express* 2021;29(3):4058–66.
- [200] Li Z, Liu T, Ren Y, Qiu S, Wang C, Wang H. Direction-sensitive detection of a spinning object using dual-frequency vortex light. *Opt Express* 2021;29(5):7453–63.
- [201] Moffitt J, Chemla Y, Smith SB, Bustamante C. Recent advances in optical tweezers. *Annu Rev Biochem* 2008;77:205–28.
- [202] Ashkin A, Dziedzic JM. Optical trapping and manipulation of viruses and bacteria. *Science* 1987;235(4795):1517–20.
- [203] Ashkin A, Dziedzic JM, Bjorkholm JE, Chu S. Observation of a single-beam gradient force optical trap for dielectric particles. *Opt Lett* 1986;11(5):288–90.
- [204] Schmiegelow CT, Schulz J, Kaufmann H, Ruster T, Poschinger UG, Schmidt KF. Transfer of optical orbital angular momentum to a bound electron. *Nat Commun* 2016;7(1):12998.
- [205] Simpson NB, Dholakia K, Allen L, Padgett MJ. Mechanical equivalence of spin and orbital angular momentum of light: an optical spanner. *Opt Lett* 1997;22(1):52–4.
- [206] Carruthers AE, Walker JS, Casey A, Orr EAJ, Reid JP. Selection and characterization of aerosol particle size using a bessel beam optical trap for single particle analysis. *PCCP* 2012;14(19):6741–8.
- [207] Garceschavez V, McGloin D, Melville H, Sibbett W, Dholakia K. Simultaneous micromanipulation in multiple planes using a self-reconstructing light beam. *Nature* 2002;419(6903):145–7.
- [208] Kim D, Tripathy SK, Li L, Kumar J. Laser-induced holographic surface relief gratings on nonlinear optical polymer films. *Appl Phys Lett* 1995;66(10):1166–8.
- [209] Moharam MG, Gaylord TK. Diffraction analysis of dielectric surface-relief gratings. *J Opt Soc Am* 1982;72(10):1385–92.
- [210] Curtis JE, Koss BA, Grier DG. Dynamic holographic optical tweezers. *Opt Commun* 2002;207(1):169–75.
- [211] Li X, Zhou Y, Cai Y, Zhang Y, Yan S, Li M, Li R, Yao B. Generation of hybrid optical trap array by holographic optical tweezers. *Front Phys* 2021;9(46):591747.
- [212] Carpenter J, Wilkinson TD. Characterization of multimode fiber by selective mode excitation. *J Lightwave Technol* 2012;30(10):1386–92.
- [213] Toyoda K, Miyamoto K, Aoki N, Morita R, Omatsu T. Using optical vortex to control the chirality of twisted metal nanostructures. *Nano Lett.* 2012;12(7):3645–9.
- [214] Ambrosio A, Marrucci L, Borbone F, Roviello A, Maddalena P. Light-induced spiral mass transport in azo-polymer films under vortex-beam illumination. *Nat Commun* 2012;3(1):989.
- [215] Khonina SN, Ustinov AV, Volotovskiy SG, Ivliev NA, Podlipnov VV. Influence of optical forces induced by paraxial vortex Gaussian beams on the formation of a microrelief on carbazole-containing azopolymer films. *Appl Opt* 2020;59(29):9185–94.
- [216] Yang L, Ji S, Xie K, Du W, Liu B, Hu Y, Li J, Zhao G, Wu D, Huang W, Liu S, Jiang H, Chu J. High efficiency fabrication of complex microtube arrays by scanning focused femtosecond laser Bessel beam for trapping/releasing biological cells. *Opt Express* 2017;25(7):8144–57.
- [217] Padgett MJ. Orbital angular momentum 25 years on. *Opt Express* 2017;25(10):11265–74.
- [218] Hell SW, Wichmann J. Breaking the diffraction resolution limit by stimulated emission: stimulated-emission-depletion fluorescence microscopy. *Opt Lett* 1994;19(11):780–2.
- [219] Yan L, Kristensen P, Ramachandran S. Vortex fibers for STED microscopy. *APL Photonics* 2018;4(2):022903.
- [220] Harke B, Keller J, Ullal CK, Westphal V, Schönlé A, Hell SW. Resolution scaling in STED microscopy. *Opt Express* 2008;16(6):4154–62.
- [221] Wang B, Shi J, Zhang T, Xu X, Cao Y, Li X. Improved lateral resolution with an annular vortex depletion beam in STED microscopy. *Opt Lett* 2017;42(23):4885–8.
- [222] Korobchevskaya K, Peres C, Li Z, Antipov A, Sheppard CJR, Diaspro A, Bianchini P. Intensity weighted subtraction microscopy approach for image contrast and resolution enhancement. *Sci Rep* 2016;6(1):25816.
- [223] Swartzlander GA. Peering into darkness with a vortex spatial filter. *Opt Lett* 2001;26(8):497–9.
- [224] Fürhapter S, Jesacher A, Bernet S, Ritsch-Marte M. Spiral interferometry. *Opt Lett* 2005;30(15):1953–5.
- [225] Serabyn E, Mawet D, Burruss R. An image of an exoplanet separated by two diffraction beam-widths from a star. *Nature* 2010;464(7291):1018–20.
- [226] Liu K, Li X, Gao Y, Cheng Y, Wang H, Qin Y. High-resolution electromagnetic vortex imaging based on Sparse Bayesian learning. *IEEE Sens J* 2017;17(21):6918–27.
- [227] Hassan MH, Sievert B, Svejda JT, Abbas AA, Jimenez-Saez A, Ahmad AM, Schubler M, Renning A, Solbach K, Kaiser T, Jakoby R, Sezgin A, Erni D. OAM mode order conversion and clutter rejection with OAM-coded RFID tags. *IEEE Access* 2020;8:218729–38.